

---

# Learning to Discretize Denoising Diffusion ODEs

---

Vinh Tong<sup>1,2</sup>, Anji Liu<sup>1,3</sup>, Trung-Dung Hoang<sup>4</sup>, Guy Van den Broeck<sup>3</sup>, Mathias Niepert<sup>1,2</sup>

<sup>1</sup>University of Stuttgart, <sup>2</sup>IMPRS-IS, <sup>3</sup>UCLA, <sup>4</sup>EPFL  
vinh.tong@ki.uni-stuttgart.de

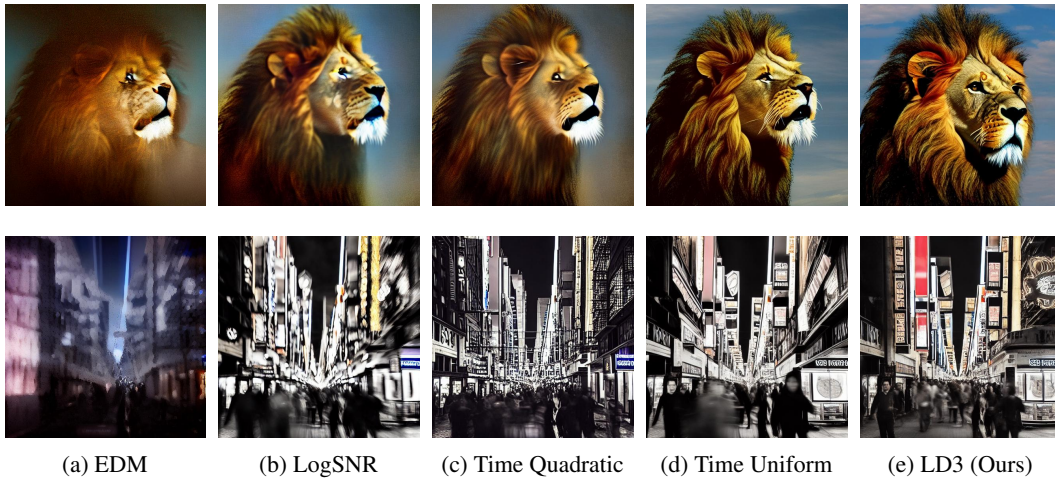


Figure 1: Comparison of time discretization strategies for Stable Diffusion [27] with 7 denoising steps. Used prompts: “A portrait of a Lion” (top) and “A lively city street at night, lit by neon signs and flickering lights, bustling with crowds and traffic noise, exudes energy and excitement” (bottom).

## Abstract

Diffusion Probabilistic Models (DPMs) are powerful generative models showing competitive performance in various domains, including image synthesis and 3D point cloud generation. However, sampling from pre-trained DPMs involves multiple neural function evaluations (NFE) to transform Gaussian noise samples into images, resulting in higher computational costs compared to single-step generative models such as GANs or VAEs. Therefore, a crucial problem is to reduce NFE while preserving generation quality. To this end, we propose LD3, a lightweight framework for learning time discretization while sampling from the diffusion ODE encapsulated by DPMs. LD3 can be combined with various diffusion ODE solvers and consistently improves performance without retraining resource-intensive neural networks. We demonstrate analytically and empirically that LD3 enhances sampling efficiency compared to distillation-based methods, without the extensive computational overhead. We evaluate our method with extensive experiments on 5 datasets, covering unconditional and conditional sampling in both pixel-space and latent-space DPMs. For example, in about 5 minutes of training on a single GPU, our method reduces the FID score from 6.63 to 2.68 on CIFAR10 (7 NFE), and in around 20 minutes, decreases the FID from 8.51 to 5.03 on class-conditional ImageNet-256 (5 NFE). LD3 complements distillation methods, offering a more efficient approach to sampling from pre-trained diffusion models.

# 1 Introduction

Diffusion Probabilistic Models (DPMs) have emerged as dominant generative models, demonstrating competitive performance across various tasks including image synthesis [2, 7, 33], text-to-image generation [5, 25, 27], 3D point cloud generation [23], and molecular generation [9]. These models aim to learn a multi-step transformation from random (e.g., Gaussian) noise to the data distribution. Despite their improved sample quality and diversity in comparison to single-step generative models like GANs [4] or VAEs [12], their multi-step nature incurs significant computational overhead.

Current DPM acceleration techniques can be divided into two main categories: distillation-based methods [19, 24, 30, 32] and advanced numerical methods [18, 20, 21, 31, 38, 41, 42]. The first method class involves updating the denoising network to encourage good generation quality with fewer time steps. While these approaches can yield notable quality improvements, re-training (or fine-tuning) the entire neural network is often costly. Additionally, distillation-based methods often encounter issues such as information loss [42] and challenges in conditional sampling [24].

The second set of approaches capitalizes on the ability to sample from DPMs by solving a corresponding diffusion Ordinary Differential Equation (ODE) [18, 20, 21, 31, 31, 38, 41, 42]. These methods treat the problem as finding better numerical solvers for diffusion ODEs, and hence require no neural network training. Solving diffusion ODEs involves a mandatory step of selecting discretization time steps, and the choice of discretization points greatly influences sample quality. However, as illustrated in Table 1, there does not exist a time discretization strategy that works well for all dataset-model-ODE solver combinations, which suggests the need for an effective yet lightweight approach to *learn good discretization time steps specific to any pre-trained DPM*.

Assuming the ODE solving pipeline is differentiable, a straightforward idea is to employ a distillation-style objective to optimize the time steps, which are inputs to the denoising neural network in DPMs and hence can be treated as trainable parameters. Specifically, we employ a teacher ODE solver that takes smaller step sizes to achieve better sample quality. The student with learnable discretized time steps is then tasked to mimic the teacher’s final output given the same input (i.e., the initial condition of the ODE). A key problem of this learning framework is the lack of capacity for the student model: it can only optimize a handful of parameters to mimic the behavior of a much stronger teacher. This leads to “underfitting” of the student, which results in suboptimal performance.

To overcome this problem, we propose a surrogate objective that is easier for the student to optimize than the ground truth distillation one. We demonstrate the validity of the proposed objective by theoretically proving its “closeness” to the original distillation objective. This is done by upper bounding the Kullback-Leibler (KL) divergence between the distribution induced by the teacher solver and the student solver that minimizes the surrogate objective. The resultant algorithm, termed **Learning to Discretize Denoising Diffusion ODEs (LD3)**, efficiently learns the time discretization by backpropagating through the ODE-solving procedure using the proposed surrogate loss. LD3 can be viewed as an additional step to further improve the sample quality of DPMs after making other design choices such as distilling the denoising model and choosing an ODE solver. Additionally, LD3 is efficient and only requires a small set of random samples from a tractable noise distribution.

Empirically, we test LD3 on both pixel space [10] and latent space DPMs [27] across various resolutions, including  $32 \times 32$  (e.g., CIFAR10 [13]),  $256 \times 256$  (e.g., LSUN-Bedroom [37], ImageNet [28]), and  $512 \times 512$  text-to-image generation [27] as well as various types of conditions (e.g., class, text prompt) [27]. LD3 performs significantly better than existing time discretization heuristics, especially with small NFE (below 10). Additionally, LD3 can be trained in 5 to 40 minutes on a single GPU.

# 2 Background

Diffusion Probabilistic Models (DPMs) [7, 33] involve a forward diffusion process that gradually converts samples following a data distribution into samples from a pre-specified noise distribution. Specifically, given a sample  $\mathbf{x}_0$  from the data distribution  $q$ , the forward process gradually perturbs it by adding Gaussian noise, which is chosen such that the distribution at time step  $T$  is a Gaussian distribution:  $\mathbf{x}_T \sim \mathcal{N}(\mathbf{0}, \sigma_T^2 \mathbf{I})$ . For any  $t \in [0, T]$ , the Gaussian transition kernel is defined as

$$q(\mathbf{x}_t | \mathbf{x}_0) = \mathcal{N}(\alpha_t \mathbf{x}_0, \sigma_t^2 \mathbf{I}),$$

where  $\alpha_t$  and  $\sigma_t$  are two noise schedule hyperparameters designed so that  $\alpha_t^2 / \sigma_t^2$  (the signal-to-noise ratio or SNR for short) is strictly decreasing with respect to  $t$ . This ensures that more information about  $\mathbf{x}_0$  is discarded as  $t$  increases.

	CIFAR10	AHQv2	LSUN-B	ImageNet		CIFAR10	AHQv2	LSUN-B	ImageNet
Time LogSNR	43.9	33.8	73.9	50.3	Time LogSNR	3.2	3.8	7.7	4.5
Time uniform	282.8	153.2	39.8	20.0	Time uniform	207.4	97.3	3.5	5.0
Time quadratic	164.8	66.4	36.0	30.7	Time quadratic	35.5	16.3	7.4	4.3
Time EDM	50.7	23.7	297.8	235.3	Time EDM	6.1	6.3	129.8	145.1
LD3 (learned)	17.7	11.5	20.2	9.9	LD3 (learned)	2.9	2.9	3.6	4.3

(a) NFE=4

(b) NFE=10

Table 1: **Different dataset-DPM pairs exhibit varying optimal time discretization.** The best, second-best, and third-best methods (measured by FID score) are distinguished by coral |, peach |, and ivory | highlighting, respectively. LSUN-B stands for LSUN-Bedroom.

To learn the data distribution  $q(\mathbf{x}_0)$ , DPMs are tasked to add back information discarded by the forward process, which results in a so-called backward process that starts from  $\mathbf{x}_T \sim q(\mathbf{x}_T)$  and moves backward through time to reconstruct  $\mathbf{x}_0$ . Specifically, a neural network  $\epsilon_\theta(\mathbf{x}_t, t)$  is trained to predict the noise added by the forward pass given  $\mathbf{x}_t$  and  $t$  by minimizing

$$\mathbb{E}_{\mathbf{x}_0, \epsilon, t} [\omega(t) \|\epsilon_\theta(\mathbf{x}_t, t) - \epsilon\|_2^2],$$

where  $\mathbf{x}_t := \alpha_t \mathbf{x}_0 + \sigma_t \epsilon$  with  $\epsilon \sim \mathcal{N}(\mathbf{0}, \mathbf{I})$  is the noisy sample at time  $t$ ,  $t \sim \mathcal{U}[0, T]$  is the time step, and  $\omega(t) \in \mathbb{R}^+$  is a time-dependent weight for time step  $t$ .  $\epsilon_\theta(\mathbf{x}_t, t)$  is a learnable deterministic function parameterized by  $\theta$  that predicts the noise added to  $\mathbf{x}_t$ .

One way to sample from a trained DPM is to first draw  $\mathbf{x}_T$  randomly and then use it as the initial condition to solve the following *diffusion ODE*, whose solution is proven to match the data distribution  $q(\mathbf{x}_0)$  if  $\epsilon_\theta(\mathbf{x}_t, t)$  is optimal [18, 20, 21, 31, 33, 38, 41, 42]:

$$\frac{\partial \mathbf{x}_t}{\partial t} = f(t) \mathbf{x}_t + \frac{g^2(t)}{2\sigma_t} \epsilon_\theta(\mathbf{x}_t, t), \text{ where } f(t) = \frac{\partial \log \alpha_t}{\partial t}, g^2(t) = \frac{\partial \sigma_t^2}{\partial t} - 2f(t)\sigma_t^2. \quad (1)$$

### 3 Learning to Discretize Denoising Diffusion ODEs

Our main goal is to reduce the computational burden of DPMs while maintaining their generation quality. In particular, we focus on the small number of neural function evaluation (NFE) regimes with at most 10 evaluations of the denoising network to generate a sample.

The ODE view of DPMs allows us to treat the problem of DPM sampling as solving a class of ODEs, where choosing the discretization points is a critical step. Although one may hope that there exists a universal discretization strategy for various DPMs, we found in Table 1 that both the structure of the DPM and the training data influence the optimal time discretization, with no single discretization strategy working well for all cases. Instead, we propose a general yet efficient algorithm to learn discretization strategies for DPMs. In the following, we first approach this problem under the framework of model distillation (Sec. 3.1). We then elaborate on a key problem of this distillation pipeline and propose a surrogate objective to significantly improve distillation performance (Sec. 3.2). Finally, we provide details of the algorithm and the training process (Sec. 3.3).

#### 3.1 Distillation-Based Learning of Discretization Strategy

Given a pre-trained denoising network  $\epsilon_\theta(\cdot, \cdot)$  and an initial state  $\mathbf{x}_T \sim \mathcal{N}(\mathbf{0}, \sigma_T^2 \mathbf{I})$  at time step  $T$ , we solve the diffusion ODE stated in Equation (1) (e.g., using the Euler or Heun’s method) by employing a sequence of time steps  $\{t_i\}_{i=0}^N$  such that  $T = t_0 > t_1 > \dots > t_N = 0$ . We denote the numerical solution of this diffusion ODE at  $t_N = 0$  as  $\Psi(\mathbf{x}_T, \{t_i\}_{i=0}^N, \epsilon_\theta)$ .

Recall that our objective is to learn the time steps  $\{t_i\}_{i=0}^N$ . To ensure their monotonicity, we encode the time steps by a monotonic function  $\tau_\xi$  parameterized by  $\xi$  such that  $\tau_\xi(i) = t_i$  ( $\forall i \in \mathbb{N}, 0 \leq i \leq N$ ).<sup>1</sup>

<sup>1</sup>More details about  $\tau_\xi$  will be discussed in Section 3.3.

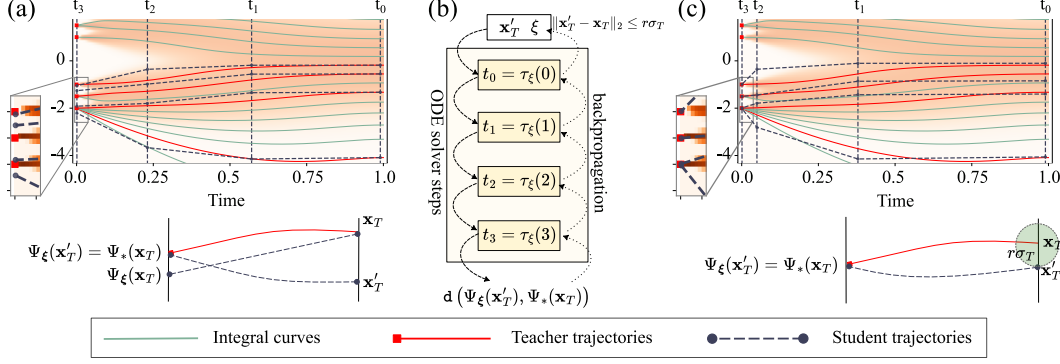


Figure 2: **Motivation and elaboration of LD3.** (a) Directly optimizing the distillation loss  $\mathcal{L}_{\text{hard}}$  leads to underfitting. (b) LD3 optimizes a surrogate objective  $\mathcal{L}_{\text{soft}}$  that allows discrepancies in the initial condition (i.e.,  $\mathbf{x}_T$ ) between the teacher solver and the student solver. (c) By optimizing the surrogate objective, LD3 learns better discretization strategies.

In the following, we simplify  $\Psi(\mathbf{x}_T, \{\tau_{\xi}(i)\}_{i=0}^N, \epsilon_{\theta})$  into  $\Psi_{\xi}(\mathbf{x}_T)$ . Additionally, we denote the distribution induced by  $\Psi_{\xi}(\mathbf{x}_T)$  as  $p_{\xi}(\mathbf{x}_0)$  (i.e., by first sample  $\mathbf{x}_T$  and then forward through  $\Psi_{\xi}(\cdot)$ ).

Define  $\Psi_*(\mathbf{x}_T, \epsilon_{\theta})$  as a teacher ODE solver that accurately solves the diffusion ODE and the distribution induced by  $\Psi_*$  as  $q(\mathbf{x}_0)$ . We aim to minimize the KL divergence between the teacher distribution  $q(\mathbf{x}_0)$  and the student distribution  $p_{\xi}(\mathbf{x}_0)$ :

$$\min_{\xi} D_{\text{KL}}(q(\mathbf{x}_0) \parallel p_{\xi}(\mathbf{x}_0)) = \min_{\xi} \mathbb{E}_{\mathbf{x}_0 \sim q(\cdot)} \left[ \log \left( \frac{q(\mathbf{x}_0)}{p_{\xi}(\mathbf{x}_0)} \right) \right]. \quad (2)$$

A straightforward approach to minimize the above objective is to do teacher forcing, i.e., to have the student ODE solver  $\Psi_{\xi}$  to mimic the teacher  $\Psi_*$ . Formally, this leads to the following objective:

$$\min_{\xi} \mathcal{L}_{\text{hard}}(\xi) := \min_{\xi} \mathbb{E}_{\mathbf{x}_T \sim \mathcal{N}(0, \sigma_T^2 \mathbf{I})} [\mathbf{d}(\Psi_{\xi}(\mathbf{x}_T), \Psi_*(\mathbf{x}_T))] \quad (3)$$

where  $\mathbf{d}(\cdot, \cdot)$  is a differentiable function that satisfies  $\forall \mathbf{x}, \mathbf{y} : \mathbf{d}(\mathbf{x}, \mathbf{y}) \geq 0$  and  $\mathbf{d}(\mathbf{x}, \mathbf{y}) = 0$  if and only if  $\mathbf{x} = \mathbf{y}$ . Some examples are squared  $l_2$  distance  $\mathbf{d}(\mathbf{x}, \mathbf{y}) = \|\mathbf{x} - \mathbf{y}\|_2^2$  and Learned Perceptual Image Patch Similarity (LPIPS) [40]. For any valid loss in the form of Equation (3), its global optimal solutions are also global optimal solutions to Equation (2).

### 3.2 Optimizing Discretization Points by Soft Teacher Forcing

Despite having the same global optimum as the KL divergence between the teacher-induced and the student-induced distribution, directly optimizing  $\mathcal{L}_{\text{hard}}(\xi)$  could lead to severe underfitting — to minimize the objective, we need to ensure  $\Psi_*(\mathbf{x}_T) = \Psi_{\xi}(\mathbf{x}_T)$  for any  $\mathbf{x}_T$ , which is hard as we are only allowed to optimize  $\xi$ , which typically contains no more than 20 parameters for student ODE solvers with low NFE. This issue is illustrated by the 1D ODE shown in Figure 2(a), where the green curves are the ground truth integral curves, and the red trajectories are from the teacher. The teacher matches the ground truth closely, as it can take fine-grained steps to solve the ODE. However, given the restriction that the student solver can only evaluate the ODE at three time steps before generating the output, an inevitable discretization error exists between the teacher and the student.

One way around this problem is to optimize the parameters of the student denoising network  $\epsilon_{\theta}$  in addition to  $\xi$ . However, this will significantly increase the sample complexity and the training time, limiting the method’s efficiency and portability.

Instead, we propose to relax the “hard” teacher forcing criterion. Specifically, for any  $\mathbf{x}_T$  and the corresponding output of the teacher  $\mathbf{x}_0 := \Psi_*(\mathbf{x}_T)$ , we only require the existence of an input  $\mathbf{x}'_T$  that is “close” to  $\mathbf{x}_T$ , such that the student’s output given  $\mathbf{x}'_T$  (i.e.,  $\Psi_{\xi}(\mathbf{x}'_T)$ ) matches  $\mathbf{x}_0$ . Formally, we define  $B(\mathbf{x}, r\sigma_T) := \{\mathbf{x}' \mid \|\mathbf{x} - \mathbf{x}'\|_2 \leq r\sigma_T\}$  as the  $L_2$  ball of radius  $r\sigma_T$  around  $\mathbf{x}$ . Again, take the 1D ODE in Figure 2(a) as an example. Although it is impossible to force the student solvers to map the same point  $\mathbf{x}_T$  to the teacher output, we can find another input  $\mathbf{x}'_T$  that maps to the teacher output  $\Psi_*(\mathbf{x}_T)$  (i.e.,  $\Psi_{\xi}(\mathbf{x}'_T)$ ). The hope is that if we can find such  $\mathbf{x}'_T$  points that are close to  $\mathbf{x}_T$ , as shown in Figure 2(c), the student solver’s distribution at  $t = 0$  still matches the teacher’s distribution well.

Formally, we relax the objective defined in Equation (3) into the following for an  $r > 0$ :

$$\min_{\xi} \mathcal{L}_{\text{soft}}(\xi) := \min_{\xi} \mathbb{E}_{\mathbf{x}_T \sim \mathcal{N}(\mathbf{0}, \sigma_T^2 \mathbf{I})} \left[ \min_{\mathbf{x}'_T \in B(\mathbf{x}_T, r\sigma_T)} d(\Psi_{\xi}(\mathbf{x}'_T), \Psi_*(\mathbf{x}_T)) \right]. \quad (4)$$

The effectiveness of this relaxed objective depends on two questions: (i) compared to  $\mathcal{L}_{\text{hard}}(\xi)$ , how much easier is it to optimize  $\mathcal{L}_{\text{soft}}(\xi)$  given the fact that we only have a handful of learnable parameters (i.e.,  $\xi$ ); (ii) whether minimizing  $\mathcal{L}_{\text{soft}}(\xi)$  leads to student distributions that have small KL divergence with the teacher distribution (i.e., the ground-truth objective in Eq. (2)).

We start by showing positive evidence to the first question — empirically, a small  $r$  suffices to ensure  $\mathcal{L}_{\text{soft}}(\xi)$  being much smaller than  $\mathcal{L}_{\text{hard}}(\xi)$ . We experiment on a pre-trained DPM [10] on AFHQv2 [1]. We optimize the discretization points (i.e.,  $\xi$ ) with respect to  $\mathcal{L}_{\text{soft}}(\xi)$  using different  $r$  and plot the training loss. We use the LPIPS distance [40] for  $d(\cdot, \cdot)$ . As shown in Figure 3, compared to  $r = 0.0$ , where  $\mathcal{L}_{\text{soft}}$  and  $\mathcal{L}_{\text{hard}}$  are identical, the loss is significantly reduced as we increase  $r$ .

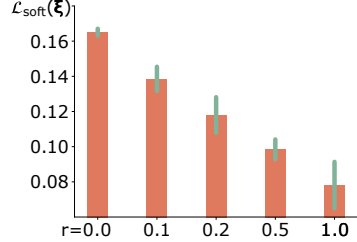


Figure 3:  $\mathcal{L}_{\text{soft}}(\xi)$  drops significantly as we increase  $r$ .

We then move on to the second question: if we can effectively minimize  $\mathcal{L}_{\text{soft}}(\xi)$ , can we establish some form of guarantee of the student in terms of its KL divergence with the teacher distribution? We answer the question in its affirmative with the following theoretical result.

**Theorem 1.** *Let  $\Psi_*$  and  $\Psi_{\xi}$  be a teacher and student ODE solver each with noise distribution  $\mathcal{N}(\mathbf{0}, \sigma_T^2 \mathbf{I}) \in \mathbb{R}^d$ , and with, respectively, distributions  $q$  and  $p_{\xi}$ . Assume both  $\Psi_*$  and  $\Psi_{\xi}$  are invertible. Let  $r > 0$ , if the objective from Equation (4) has an optimal solution  $\xi^*$  for  $r$  with objective value 0, we have*

$$D_{\text{KL}}(q(\mathbf{x}) \parallel p_{\xi^*}(\mathbf{x})) \leq \frac{r^2}{2} + r\sqrt{d+1} + \mathbb{E}_{\mathbf{x} \sim q(\mathbf{x})} [|C(\Psi_*(\mathbf{x})) - C(\Psi_{\xi^*}(\mathbf{x}))|],$$

where  $C(\Psi_{\xi^*}(\mathbf{x})) = \log |\det J_{\Psi_{\xi^*}}(\Psi_{\xi^*}^{-1}(\mathbf{x}))|$ .

The proof is provided in Appendix A.1. Intuitively, the theorem states that, if we can find an optimal solution  $\xi^*$  that minimizes  $\mathcal{L}_{\text{soft}}$ , then the KL divergence between the teacher (i.e.,  $q(\mathbf{x})$ ) and the student (i.e.,  $p_{\xi^*}(\mathbf{x})$ ) can be upper bounded. The first two terms depend mainly on  $r$  and the square root of the dimensionality:  $\sqrt{d+1}$ . Since  $r$  is chosen to be quite small (e.g., 0.19 for CIFAR10, 4 NFE), the first two terms are effectively tight in practice. While it is hard to establish an analytic bound for the third term, we conduct numerical evaluations to estimate its magnitude in practice and observe that it reduces with  $r$ . See Appendix A.2 for more details.

### 3.3 Practical Implementation

Now that we have justified the effectiveness of  $\mathcal{L}_{\text{soft}}(\xi)$ , we are left with the question of how to optimize it in practice. This is achieved by treating  $\mathcal{L}_{\text{soft}}(\xi)$  as jointly optimizing  $\xi$  and  $\mathbf{x}'_T$  with the constraint that  $\mathbf{x}'_T$  is within the  $r$ -ball of  $\mathbf{x}_T$ :

$$\mathcal{L}(\xi, \mathbf{x}'_T) := \mathbb{E}_{\mathbf{x}_T \sim \mathcal{N}(\mathbf{0}, \sigma_T^2 \mathbf{I})} [\text{LPIPS}(\Psi_{\xi}(\mathbf{x}'_T), \Psi_*(\mathbf{x}_T))], \text{ subject to } \mathbf{x}'_T \in B(\mathbf{x}_T, r\sigma_T). \quad (5)$$

Note that we choose  $d := \text{LPIPS}$  [40] as the distance metric in our setting. LPIPS is also a common choice in many distillation-based models [30, 32]. As illustrated in Figure 2(b), given an input-output pair  $(\mathbf{x}_T, \Psi_*(\mathbf{x}_T))$  from the teacher, we forward through the student ODE solver steps with learnable parameters  $\xi$  and  $\mathbf{x}'_T$ . Backpropagation is then performed to get the gradients w.r.t.  $\text{LPIPS}(\Psi_{\xi}(\mathbf{x}'_T), \Psi_*(\mathbf{x}_T))$ . Finally, we use projected SGD to enforce the constraint on  $\mathbf{x}'_T$  and use SGD to update  $\xi$ . Specifically, let  $\mathbf{x}_T$  be the center of a  $r$ -sphere and  $\mathbf{x}'_T$  a point. Then the projection of  $\mathbf{x}'_T$ , which is the intersection of the line between  $\mathbf{x}_T$  and  $\mathbf{x}'_T$  with the sphere's surface, can be computed as  $\mathbf{x}_p := \mathbf{x}_T + r \frac{\mathbf{x}'_T - \mathbf{x}_T}{\|\mathbf{x}'_T - \mathbf{x}_T\|_2}$ .

**Parameterization.** Starting from a trainable vector  $\xi \in \mathbb{R}^{N+1}$ , we model  $\tau_{\xi}(i)$  as a strictly monotonically decreasing function using a cumulative softmax function, followed by renormalization to

the range  $[t_{\min}, T]$ :

$$\tau_{\xi}(i) := \frac{\tau'_{\xi}(i) - \tau'_{\xi_{\min}}}{\tau'_{\xi_{\max}} - \tau'_{\xi_{\min}}}(T - t_{\min}) + t_{\min}, \quad \text{where} \quad \tau'_{\xi}(i) = \sum_{n=i}^N \text{softmax}(\xi)[n].$$

Here,  $t_{\min}$  is often utilized in training and sampling as a substitute for 0 in the diffusion model to mitigate numerical instability problems [10, 32].

During training, DPMs denoise images generated from real data, whereas, during inference, they use predictions from previous steps, causing discrepancies that can lead to errors [15, 26]. As suggested by [15], we learn decoupled time steps  $t_i^c$ , used as input to the denoising model, while  $t_i$  determines the solver’s step size. We parameterize  $t_i^c$  as  $\tau'_{\xi}(i) := \tau_{\xi}(i) + \xi_i^c$ . For notation simplicity, we still use  $\Psi_{\xi}$  to refer to the student solver with additional decoupled time step variables.

---

**Algorithm 1** LD3

---

**Require:** Student solver  $\Psi_{\xi}$ , teacher solver  $\Psi_*$ , and  $r$

- 1:  $\mathcal{D} \leftarrow \{(\mathbf{x}'_T, \mathbf{x}_T, \Psi_*(\mathbf{x}_T)) \mid \mathbf{x}_T \sim \mathcal{N}(\mathbf{0}, \sigma_T^2), \mathbf{x}'_T = \mathbf{x}_T\}$  ▷ Generate data  $\mathcal{D}$
- 2: **while** not converged **do**
- 3:  $(\mathbf{x}'_T, \mathbf{x}_T, \Psi_*(\mathbf{x}_T)) \sim \mathcal{D}$
- 4:  $\mathcal{L}(\xi, \xi^c, \mathbf{x}'_T) = \text{LPIPS}(\Psi_{\xi, \xi^c}(\mathbf{x}'_T), \Psi_*(\mathbf{x}_T))$  subject to  $\mathbf{x}'_T \in B(\mathbf{x}_T, r\sigma_T)$
- 5: Update  $\xi, \xi^c$ , and  $\mathbf{x}'_T$  using the corresponding gradients  $\nabla \mathcal{L}(\xi, \xi^c, \mathbf{x}'_T)$
- 6:  $\mathbf{x}'_T \leftarrow \mathbf{x}'_T + \mathbb{1}[\|\mathbf{x}'_T - \mathbf{x}_T\|_2 > r] \cdot r \frac{\mathbf{x}'_T - \mathbf{x}_T}{\|\mathbf{x}'_T - \mathbf{x}_T\|_2}$  ▷ Projected SGD
- 7: Update  $\mathcal{D}$  with the new  $\mathbf{x}'_T$
- 8: **end while**

---

**Training.** The final LD3 algorithm is shown in Algorithm 1. In line 1, we first generate training samples by first sample  $\mathbf{x}_T \sim \mathcal{N}(\mathbf{0}, \sigma_T \mathbf{I})$  and then compute the corresponding teacher outputs  $\Psi_*(\mathbf{x}_T)$ . Initially, the same starting samples are used for both the student and the teacher (i.e.,  $\mathbf{x}'_T = \mathbf{x}_T$ ), resulting in a dataset  $\mathcal{D} = \{(\mathbf{x}'_T, \mathbf{x}_T, \Psi_*(\mathbf{x}_T))\}$ . In every iteration, we first compute the objective shown in Equation (5) (line 4), and then apply gradient-based updates to  $\xi$  and  $\mathbf{x}'_T$  (line 5). An additional projected SGD step is applied to  $\mathbf{x}'_T$  to bound the distance between  $\mathbf{x}'_T$  and  $\mathbf{x}_T$  (line 6). The algorithm terminates after convergence.

Since computing  $\Psi_{\xi}(\mathbf{x}'_T)$  involves evoking the denoising network  $\epsilon_{\theta}$  multiple times, naively storing all intermediate outputs for efficient backpropagation would lead to memory overhead that scales linearly w.r.t. NFE. To reduce the memory overhead, we use the rematerialization technique proposed in [34] to only cache the intermediate  $\mathbf{x}_t$ . This leads to an almost constant memory overhead w.r.t. NFE. Please refer to Appendix B.3 for details.

## 4 Related work

One class of well-established approaches to speed up DPMs is to distill high-quality denoising networks that require many function evaluations into models that demand much fewer steps with the minimum possible performance drop [3, 24, 30]. However, it entails costly training [19, 22, 24, 32] before they can be used for sampling. Some even require pre-generating hundreds of thousands to millions of images before training [24, 36].

Orthogonal to fine-tuning the denoising network, another direction is to design advanced solvers tailored to diffusion ODEs (i.e., Equation (1)) [18, 20, 21, 31, 38, 41]. The key insight is that the discretization error accumulated in the backward sampling process can significantly harm the quality of generated images when the NFE becomes small. Hence, effective ODE solvers are needed to reduce it. For example, exponential integrator-based ODE solvers [8, 20, 21, 38] enjoy faster convergence compared to black box ODE solvers [10]. Moreover, [21, 39, 42] propose some modified yet equivalent *diffusion ODE* that enjoys better numerical solutions.

Despite having minimal computation overhead and being easy to use in a plug-and-play fashion, these methods still fall short in performance compared to distillation-based techniques. This gives rise to the third family of approaches which seek to identify components in DPMs that are performance-critical while being easily/efficiently optimized such as the prediction type of the neural network [17, 42], or order of Taylor expansion [17]. Among these components, time discretization points are considered important [17, 29, 34, 35, 43]. Zhou et al. [43] propose a trainable framework for optimizing intermediate time steps in single-step solvers. Watson et al. [34, 35] propose the Differentiable



Table 2: **FID score comparison on LSUN-Bedroom 256×256.** We compare LD3 with best-performed discretization baselines (Best) among *time uniform*, *time quadratic*, *time EDM*, and *time logSNR*.

Solver	Method	NFE=4	NFE=5	NFE=6	NFE=7	NFE=8	NFE=9	NFE=10
Uni_PC(2M) [41]	Best	35.97	13.88	6.57	4.56	<b>3.96</b>	3.74	<b>3.54</b>
	LD3	<b>20.15</b> $\pm$ 1.10	<b>9.09</b> $\pm$ 0.42	<b>4.98</b> $\pm$ 0.10	<b>4.18</b> $\pm$ 0.15	<b>4.01</b> $\pm$ 0.05	<b>3.61</b> $\pm$ 0.04	<b>3.60</b> $\pm$ 0.08
DPM_Solver++(2M) [21]	Best	47.64	18.64	8.50	5.16	4.24	<b>3.84</b>	<b>3.62</b>
	LD3	<b>28.83</b> $\pm$ 0.16	<b>12.17</b> $\pm$ 0.68	<b>5.83</b> $\pm$ 0.15	<b>4.16</b> $\pm$ 0.04	<b>3.71</b> $\pm$ 0.03	<b>3.77</b> $\pm$ 0.07	3.81 $\pm$ 0.11
iPNDM(2M) [38]	Best	11.93	6.38	5.08	<b>4.39</b>	4.17	<b>3.81</b>	<b>3.69</b>
	LD3	<b>8.48</b> $\pm$ 0.11	<b>5.93</b> $\pm$ 0.11	<b>4.52</b> $\pm$ 0.17	<b>4.31</b> $\pm$ 0.17	<b>3.87</b> $\pm$ 0.07	<b>3.84</b> $\pm$ 0.07	<b>3.59</b> $\pm$ 0.10

Diffusion Sampler Search method, which aims to improve the Kernel Inception Score by optimizing time discretization. However, their method requires a large amount of training samples and needs over 50k iterations with batch size 512 to converge. In comparison, our method only requires 200 iterations each with batch size 1 or 2. Concurrent to our work, Sabour et al. [29] aim to optimize the time discretization points toward a KL-divergence Upper Bound objective (KLUB). Unlike our objective, optimizing KLUB is difficult due to its high variance. Moreover, as shown in Appendix C.1, LD3 obtains lower FID scores in the low-NFE regimes and comparable scores in the high-NFE regime while being more efficient (see Section 5.4).

## 5 Experiment

We show that LD3 can learn good discretization on various datasets and diffusion models (Sec. 5.2). We then conduct ablation studies to justify the effectiveness of the proposed surrogate objective (Sec. 5.3). Finally, we show that LD3 is lightweight, which allows us to optimize time discretization in less than an hour on a single GPU for high-resolution image DPMs (Sec. 5.4).

### 5.1 Setting

We evaluate various pre-trained diffusion models on several datasets: CIFAR10 (32×32) [13], FFHQ (64×64) [11], AFHQv2 (64×64) [1], LSUN-Bedroom (256×256) [37], and class-conditional ImageNet (256×256) [28] with a guidance scale of 2.0. We test both pixel space [10] and latent space [27] DPMs. Further, we present qualitative results for Stable Diffusion v1.4 [27] at 512×512 pixels with a guidance scale of 7.5 in Figure 1 and Appendix C.4.

We primarily assess LD3 using advanced diffusion ODE solvers: DPM\_solver++ [21], Uni\_PC [41], and iPNDM [38]. We also test LD3 using Euler, a standard black-box ODE solver. Our learned discretization method is compared against common ones such as *time uniform* [7, 21], *time quadratic* [31], *time EDM* [10], and *time logSNR* (uniform in  $\lambda$ ) [38]. Details are provided in Appendix B.2. We also compare our model with a concurrent work [29] on ImageNet (Tab. 3), CIFAR10, and AFHQv2 (Appx. C.1).

We draw 50K samples for evaluation using the FID score [6], where lower scores indicate better quality. For CIFAR10, FFHQ, and AFHQv2, we use 100 samples for training and validation, respectively. The models are trained for 7 epochs with a batch size of 2. We report the average and standard deviation over 3 random seeds. We set  $r$  proportional to the dimensionality  $d$  and inversely proportional to the squared NFE:  $r = \gamma \times \frac{d}{\text{NFE}^2}$ , where  $\gamma = 0.001$  in all experiments.

For Latent Diffusion [27] on ImageNet and LSUN-Bedroom, we use 100 samples for both training and validation, reporting the same statistical measures with 3 random seeds, with training conducted over 5 epochs. For Stable Diffusion [27], we randomly select five prompts from the MSCOCO dataset [16] and generate 10 training pairs (half for training and half for validation) for each prompt. We train Stable Diffusion for 5 epochs. Since baseline discretization heuristics are deterministic, we do not run them multiple times or report standard deviation. Details of experiment settings can be found in Appendix B.

### 5.2 Main Results

Figure 5 presents the overall results of different solvers on the three pixel space datasets. Generally, LD3 significantly enhances generation quality across all solvers and datasets. Notably, our method can improve the performance of the black-box solver Euler beyond that of advanced solvers in

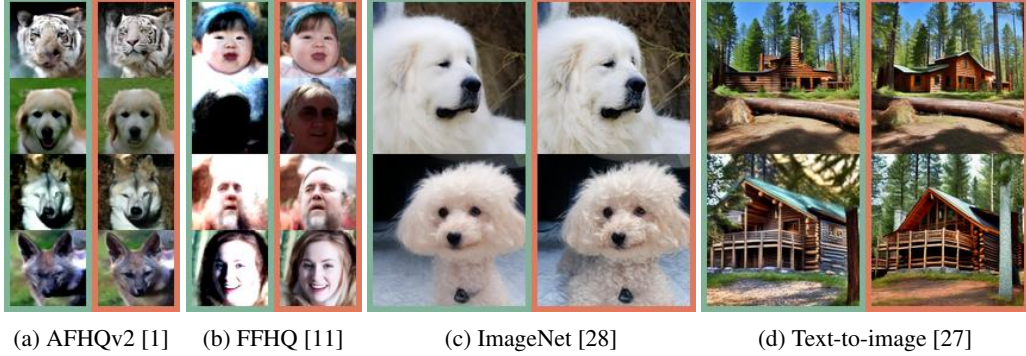


Figure 4: **Qualitative results.** We compare LD3 (coral boxes-right) with best baseline discretization (light teal boxes-left) on random images for pixel space DPMs ((a) and (b)), and latent space DPMs ((c) and (d)). We use Uni\_PC (2M) [41] solver with 5, 4, and 6 NFE for (a), (b), and (d), respectively. For (c), we use DPM\_Solver++ (2M) [21] with 8 NFE. In (d), we use the prompt: "A rustic log cabin nestled in a pine forest, surrounded by towering trees."

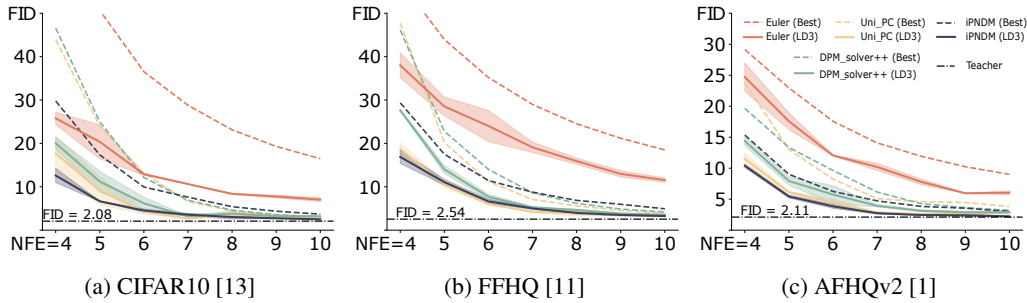


Figure 5: **Evaluation of pixel space diffusion models.** We utilize pre-trained models from [10] on three datasets CIFAR10 [13] (a), FFHQ [11] (b), and AFHQv2 [1] (c) and report the FID scores for various NFE ranging from 4 to 10. Results are averaged over 3 runs, with standard error reported. We use order = 3 for DPM\_Solver++, Uni\_PC, and iPNM. In most cases, LD3 has better FID scores compared to the best baseline discretization strategy.

scenarios with limited NFE. For instance, on CIFAR10 with 4 NFE, LD3 improves Euler’s FID from 67.82 to 25.78, surpassing the best advanced solver, iPNM, which has an FID of 29.78.

For latent space diffusion models, we evaluate our performance against the best discretization methods using Latent Diffusion models [27] trained on LSUN-Bedroom [37] and ImageNet [28], as reported in Table 3. Our model consistently outperforms or matches the best baseline models. Additionally, compared to the concurrent work AYS [29], which reports results at 10 NFE for DPM\_solver++ on ImageNet, LD3 achieves a comparable FID with only 8 NFE (4.37 versus 4.31). Notably, our model requires significantly less training time compared to AYS, as discussed in Section 5.4.

We test LD3 in high NFE regimes on the FFHQ dataset. As shown in Figure 7, even with 8-20 NFE, which are not targeted primarily by LD3, we achieve better performance compared to all baselines.

Table 3: **FID score comparison on ImageNet 256×256.** We compare LD3 with best-performed discretization baselines (Best) among *time uniform*, *time quadratic*, *time EDM*, *time logSNR*, and a concurrent work to ours (denoted AYS, the result is taken from [29]).

Solver	Method	NFE=4	NFE=5	NFE=6	NFE=7	NFE=8	NFE=9	NFE=10
Uni_PC(2M) [41]	Best	20.01	8.51	5.92	5.17	4.61	<b>4.32</b>	<b>4.32</b>
	LD3	<b>9.89±0.06</b>	<b>5.03±0.17</b>	<b>4.46±0.06</b>	<b>4.32±0.00</b>	<b>4.33±0.07</b>	<b>4.27±0.07</b>	<b>4.31±0.01</b>
DPM_Solver++(2M) [21]	Best	26.07	11.91	7.51	5.95	5.42	5.01	4.77
	AYS	N/A	N/A	N/A	N/A	N/A	N/A	<b>4.31</b>
	LD3	<b>16.92±0.13</b>	<b>6.74±0.05</b>	<b>4.74±0.08</b>	<b>4.44±0.05</b>	<b>4.37±0.05</b>	<b>4.37±0.06</b>	4.46±0.03
iDNPM(2M) [38]	Best	13.86	7.80	6.03	5.35	5.10	4.97	4.66
	LD3	<b>9.19±0.20</b>	<b>6.03±0.02</b>	<b>5.09±0.04</b>	<b>4.68±0.04</b>	<b>4.62±0.07</b>	<b>4.57±0.02</b>	<b>4.55±0.03</b>



### 5.3 Ablation Study

We investigate the importance of different components in our model as shown in Table 4. Initially, we compare variants with and without training  $\xi^c$  (cf. the decoupling technique described in Section 3.3) and then examine the effects of other factors on performance. This is particularly important because the variant without  $\xi^c$  is easily integrated into any ODE samplers, making a detailed study of its behavior beneficial to the community. We observe that  $\xi^c$  significantly contributes to the performance of LD3, which is expected as it effectively doubles the number of trainable parameters. For both versions, optimizing  $\mathcal{L}_{\text{hard}}$  results in worse performance compared to optimizing  $\mathcal{L}_{\text{soft}}$ . For instance, with NFE=5, using  $\mathcal{L}_{\text{soft}}$  improves the FID score by 18% (from 12.83 to 10.56). The effect of  $\mathcal{L}_{\text{soft}}$  is more pronounced without  $\xi^c$ ; with the same NFE,  $\mathcal{L}_{\text{soft}}$  boosts the FID by 15% (from 16.39 to 13.95).

Table 4: **Ablation study on FFHQ [11] dataset.** We conduct the experiment with Uni\_PC Solver (2M).

Model variants	NFE=4	NFE=5	NFE=6	NFE=7	NFE=8
Full setting	<b>18.72</b> $\pm$ 1.27	<b>10.56</b> $\pm$ 0.72	<b>5.99</b> $\pm$ 0.07	<b>4.23</b> $\pm$ 0.18	<b>3.85</b> $\pm$ 0.64
w/ $\xi^c$					
w/ $\mathcal{L}_{\text{hard}}$	19.49 $\pm$ 0.10	12.83 $\pm$ 1.33	7.15 $\pm$ 0.68	4.35 $\pm$ 0.07	4.13 $\pm$ 0.78
w/ L2	21.82 $\pm$ 0.47	15.61 $\pm$ 2.39	12.89 $\pm$ 0.88	12.18 $\pm$ 0.68	10.16 $\pm$ 0.52
Full setting	<b>19.82</b> $\pm$ 0.19	<b>13.95</b> $\pm$ 0.33	<b>10.46</b> $\pm$ 0.33	<b>7.32</b> $\pm$ 0.49	<b>5.65</b> $\pm$ 0.72
w/o $\xi^c$					
w/ $\mathcal{L}_{\text{hard}}$	22.85 $\pm$ 0.05	16.39 $\pm$ 0.28	12.42 $\pm$ 0.24	9.10 $\pm$ 0.29	7.11 $\pm$ 0.90
w/ L2	25.72 $\pm$ 0.05	18.51 $\pm$ 0.12	15.17 $\pm$ 0.25	13.04 $\pm$ 0.37	10.76 $\pm$ 0.16

### 5.4 Efficiency and Performance

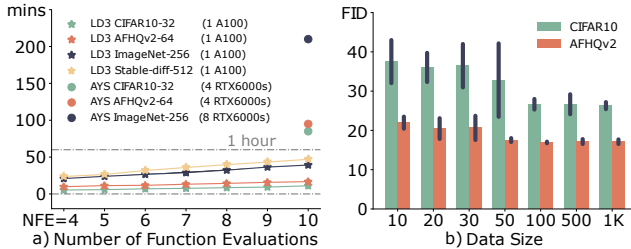


Figure 6: (a) Training time for LD3 and AYS [29] on various NFE; (b) The effect of data size on model performance (FID) is evaluated with 5K samples, DPM\_Solver++(3M), NFE=4.

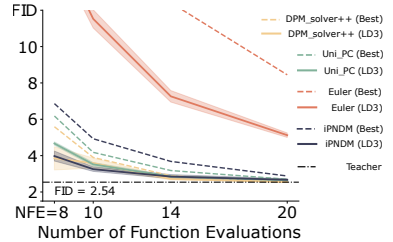


Figure 7: Performance of LD3 and baseline discretization methods on large NFE regimes.

We also evaluate the efficiency of our model. LD3 demonstrates significantly faster training times compared to AYS [29]. As shown in Figure 6 (a), LD3 can be optimized in less than an hour on a single GPU, while AYS typically requires several hours on multiple GPUs. For instance, at 10 NFE, our model needs approximately 36 minutes on a single NVIDIA A100 GPU, whereas AYS requires 3 to 4 hours on 8 NVIDIA RTX6000s.

We generally only need 100 teacher noise target pairs for training and validation. Figure 6 (b) demonstrates that increasing the training size reduces the FID score. Since the performance plateaus at around 100 samples, we use  $\sim$ 100 samples in practice to balance performance and efficiency.

## 6 Conclusion and Limitations

In conclusion, we introduced LD3, a lightweight framework designed to reduce computational costs when sampling from pre-trained DPMs. LD3 learns time discretization for ODE sampling, significantly lowering the NFE needed to generate high-quality images with minimal training overhead. Our experiments across various datasets demonstrate that LD3 consistently improves sampling quality. For instance, LD3 reduced the FID score on CIFAR10 (5 NFE) from 20.52 to 6.66 with 5 minutes of training on a GPU. These results indicate that LD3 provides a more efficient approach to sampling from pre-trained diffusion models, with promising applications in image synthesis and beyond.

**Limitation and broader impact.** Despite significant performance improvements for a few NFE, LD3 still falls short of distillation-based methods regarding sample quality. Additionally, our model necessitates a differentiable solver, which may not always be feasible. Using LD3 with advanced diffusion ODE solvers to generate fake content could also exacerbate the potential risks of LD3 being used for malicious purposes.

## **Acknowledgements**

This work was funded in part by Deutsche Forschungsgemeinschaft (DFG, German Research Foundation) under Germany's Excellence Strategy - EXC 2075 – 390740016, the DARPA PTG Program under award HR00112220005, the DARPA ANSR program under award FA8750-23-2-0004, and the NSF grant #IIS-1943641. We acknowledge the support of the Stuttgart Center for Simulation Science (SimTech). VT and MN thank IMPRS-IS (International Max Planck Research School for Intelligent Systems) for the support.

## References

- [1] Yunjey Choi, Youngjung Uh, Jaejun Yoo, and Jung-Woo Ha. Stargan v2: Diverse image synthesis for multiple domains. In *Proceedings of the IEEE/CVF conference on computer vision and pattern recognition*, pages 8188–8197, 2020.
- [2] Prafulla Dhariwal and Alexander Nichol. Diffusion models beat gans on image synthesis. *Advances in neural information processing systems*, 34:8780–8794, 2021.
- [3] Ying Fan and Kangwook Lee. Optimizing ddpn sampling with shortcut fine-tuning. *arXiv preprint arXiv:2301.13362*, 2023.
- [4] Ian Goodfellow, Jean Pouget-Abadie, Mehdi Mirza, Bing Xu, David Warde-Farley, Sherjil Ozair, Aaron Courville, and Yoshua Bengio. Generative adversarial nets. *Advances in neural information processing systems*, 27, 2014.
- [5] Shuyang Gu, Dong Chen, Jianmin Bao, Fang Wen, Bo Zhang, Dongdong Chen, Lu Yuan, and Baining Guo. Vector quantized diffusion model for text-to-image synthesis. In *Proceedings of the IEEE/CVF Conference on Computer Vision and Pattern Recognition*, pages 10696–10706, 2022.
- [6] Martin Heusel, Hubert Ramsauer, Thomas Unterthiner, Bernhard Nessler, and Sepp Hochreiter. Gans trained by a two time-scale update rule converge to a local nash equilibrium. *Advances in neural information processing systems*, 30, 2017.
- [7] Jonathan Ho, Ajay Jain, and Pieter Abbeel. Denoising diffusion probabilistic models. *Advances in Neural Information Processing Systems*, 33:6840–6851, 2020.
- [8] Marlis Hochbruck and Alexander Ostermann. Exponential integrators. *Acta Numerica*, 19:209–286, 2010.
- [9] Emiel Hoogeboom, Victor Garcia Satorras, Clément Vignac, and Max Welling. Equivariant diffusion for molecule generation in 3d. In *International conference on machine learning*, pages 8867–8887. PMLR, 2022.
- [10] Tero Karras, Miika Aittala, Timo Aila, and Samuli Laine. Elucidating the design space of diffusion-based generative models. *Advances in Neural Information Processing Systems*, 35:26565–26577, 2022.
- [11] Tero Karras, Samuli Laine, and Timo Aila. A style-based generator architecture for generative adversarial networks. In *Proceedings of the IEEE/CVF conference on computer vision and pattern recognition*, pages 4401–4410, 2019.
- [12] Diederik Kingma, Tim Salimans, Ben Poole, and Jonathan Ho. Variational diffusion models. *Advances in neural information processing systems*, 34:21696–21707, 2021.
- [13] Alex Krizhevsky, Geoffrey Hinton, et al. Learning multiple layers of features from tiny images. 2009.
- [14] Ravi Kumar, Manish Purohit, Zoya Svitkina, Erik Vee, and Joshua Wang. Efficient rematerialization for deep networks. *Advances in Neural Information Processing Systems*, 32, 2019.
- [15] Mingxiao Li, Tingyu Qu, Wei Sun, and Marie-Francine Moens. Alleviating exposure bias in diffusion models through sampling with shifted time steps. *arXiv preprint arXiv:2305.15583*, 2023.
- [16] Tsung-Yi Lin, Michael Maire, Serge Belongie, Lubomir Bourdev, Ross Girshick, James Hays, Pietro Perona, Deva Ramanan, C. Lawrence Zitnick, and Piotr Dollár. Microsoft coco: Common objects in context, 2015.
- [17] Enshu Liu, Xuefei Ning, Huazhong Yang, and Yu Wang. A unified sampling framework for solver searching of diffusion probabilistic models. *arXiv preprint arXiv:2312.07243*, 2023.

- [18] Luping Liu, Yi Ren, Zhijie Lin, and Zhou Zhao. Pseudo numerical methods for diffusion models on manifolds. *arXiv preprint arXiv:2202.09778*, 2022.
- [19] Xingchao Liu, Chengyue Gong, and Qiang Liu. Flow straight and fast: Learning to generate and transfer data with rectified flow. *arXiv preprint arXiv:2209.03003*, 2022.
- [20] Cheng Lu, Yuhao Zhou, Fan Bao, Jianfei Chen, Chongxuan Li, and Jun Zhu. Dpm-solver: A fast ode solver for diffusion probabilistic model sampling in around 10 steps. *Advances in Neural Information Processing Systems*, 35:5775–5787, 2022.
- [21] Cheng Lu, Yuhao Zhou, Fan Bao, Jianfei Chen, Chongxuan Li, and Jun Zhu. Dpm-solver++: Fast solver for guided sampling of diffusion probabilistic models. *arXiv preprint arXiv:2211.01095*, 2022.
- [22] Eric Luhman and Troy Luhman. Knowledge distillation in iterative generative models for improved sampling speed. *arXiv preprint arXiv:2101.02388*, 2021.
- [23] Shitong Luo and Wei Hu. Diffusion probabilistic models for 3d point cloud generation. In *Proceedings of the IEEE/CVF Conference on Computer Vision and Pattern Recognition*, pages 2837–2845, 2021.
- [24] Chenlin Meng, Robin Rombach, Ruiqi Gao, Diederik Kingma, Stefano Ermon, Jonathan Ho, and Tim Salimans. On distillation of guided diffusion models. In *Proceedings of the IEEE/CVF Conference on Computer Vision and Pattern Recognition*, pages 14297–14306, 2023.
- [25] Alex Nichol, Prafulla Dhariwal, Aditya Ramesh, Pranav Shyam, Pamela Mishkin, Bob McGrew, Ilya Sutskever, and Mark Chen. Glide: Towards photorealistic image generation and editing with text-guided diffusion models. *arXiv preprint arXiv:2112.10741*, 2021.
- [26] Mang Ning, Enver Sangineto, Angelo Porrello, Simone Calderara, and Rita Cucchiara. Input perturbation reduces exposure bias in diffusion models. *arXiv preprint arXiv:2301.11706*, 2023.
- [27] Robin Rombach, Andreas Blattmann, Dominik Lorenz, Patrick Esser, and Björn Ommer. High-resolution image synthesis with latent diffusion models. In *Proceedings of the IEEE/CVF conference on computer vision and pattern recognition*, pages 10684–10695, 2022.
- [28] Olga Russakovsky, Jia Deng, Hao Su, Jonathan Krause, Sanjeev Satheesh, Sean Ma, Zhiheng Huang, Andrej Karpathy, Aditya Khosla, Michael Bernstein, et al. Imagenet large scale visual recognition challenge. *International journal of computer vision*, 115:211–252, 2015.
- [29] Amirmojtaba Sabour, Sanja Fidler, and Karsten Kreis. Align your steps: Optimizing sampling schedules in diffusion models. *arXiv preprint arXiv:2404.14507*, 2024.
- [30] Tim Salimans and Jonathan Ho. Progressive distillation for fast sampling of diffusion models. *arXiv preprint arXiv:2202.00512*, 2022.
- [31] Jiaming Song, Chenlin Meng, and Stefano Ermon. Denoising diffusion implicit models. *arXiv preprint arXiv:2010.02502*, 2020.
- [32] Yang Song, Prafulla Dhariwal, Mark Chen, and Ilya Sutskever. Consistency models. *arXiv preprint arXiv:2303.01469*, 2023.
- [33] Yang Song, Jascha Sohl-Dickstein, Diederik P Kingma, Abhishek Kumar, Stefano Ermon, and Ben Poole. Score-based generative modeling through stochastic differential equations. *arXiv preprint arXiv:2011.13456*, 2020.
- [34] Daniel Watson, William Chan, Jonathan Ho, and Mohammad Norouzi. Learning fast samplers for diffusion models by differentiating through sample quality. *arXiv preprint arXiv:2202.05830*, 2022.
- [35] Daniel Watson, Jonathan Ho, Mohammad Norouzi, and William Chan. Learning to efficiently sample from diffusion probabilistic models. *arXiv preprint arXiv:2106.03802*, 2021.

- [36] Tianwei Yin, Michaël Gharbi, Richard Zhang, Eli Shechtman, Fredo Durand, William T Freeman, and Taesung Park. One-step diffusion with distribution matching distillation. *arXiv preprint arXiv:2311.18828*, 2023.
- [37] Fisher Yu, Ari Seff, Yinda Zhang, Shuran Song, Thomas Funkhouser, and Jianxiong Xiao. Lsun: Construction of a large-scale image dataset using deep learning with humans in the loop. *arXiv preprint arXiv:1506.03365*, 2015.
- [38] Qinsheng Zhang and Yongxin Chen. Fast sampling of diffusion models with exponential integrator. *arXiv preprint arXiv:2204.13902*, 2022.
- [39] Qinsheng Zhang, Jiaming Song, and Yongxin Chen. Improved order analysis and design of exponential integrator for diffusion models sampling. *arXiv preprint arXiv:2308.02157*, 2023.
- [40] Richard Zhang, Phillip Isola, Alexei A Efros, Eli Shechtman, and Oliver Wang. The unreasonable effectiveness of deep features as a perceptual metric. In *CVPR*, 2018.
- [41] Wenliang Zhao, Lujia Bai, Yongming Rao, Jie Zhou, and Jiwen Lu. Unipc: A unified predictor-corrector framework for fast sampling of diffusion models. *arXiv preprint arXiv:2302.04867*, 2023.
- [42] Kaiwen Zheng, Cheng Lu, Jianfei Chen, and Jun Zhu. Dpm-solver-v3: Improved diffusion ode solver with empirical model statistics. *Advances in Neural Information Processing Systems*, 36, 2024.
- [43] Zhenyu Zhou, Defang Chen, Can Wang, and Chun Chen. Fast ode-based sampling for diffusion models in around 5 steps. *arXiv preprint arXiv:2312.00094*, 2023.

## A Analytical proofs

### A.1 Proof of theorem

**Theorem 1.** Let  $\Psi_*$  and  $\Psi_\xi$  be a teacher and student ODE solver each with noise distribution  $\mathcal{N}(\mathbf{0}, \sigma_T^2 \mathbf{I})$ ,  $\mathbf{0} \in \mathbb{R}^d$ , and with, respectively, distributions  $q$  and  $p_\xi$ . Assume both  $\Psi_*$  and  $\Psi_\xi$  are invertible. Let  $r > 0$ , if the objective from Equation (4) has an optimal solution  $\xi^*$  for  $r$  with objective value 0, we have

$$D_{\text{KL}}(q(\mathbf{x}) \parallel p_{\xi^*}(\mathbf{x})) \leq \frac{r^2}{2} + r\sqrt{d+1} + \mathbb{E}_{\mathbf{x} \sim q(\mathbf{x})} [|C(\Psi_*(\mathbf{x})) - C(\Psi_{\xi^*}(\mathbf{x}))|],$$

where  $C(\Psi_{\xi^*}(\mathbf{x})) = \log |\det J_{\Psi_{\xi^*}}(\Psi_{\xi^*}^{-1}(\mathbf{x}))|$ .

*Proof.* By assuming the invertibility of the solvers and the loss of Equation (4) having an optimal (zero loss and satisfying all  $r$ -ball constraints) solution  $\xi^*$ , we have for every  $\mathbf{x} \sim q(\mathbf{x})$  exactly one  $\mathbf{b}$  with  $\Psi_*^{-1}(\mathbf{x}) = \mathbf{b}$  and exactly one corresponding  $\mathbf{a}$  with  $\Psi_{\xi^*}^{-1}(\mathbf{x}) = \mathbf{a}$ . Moreover, by definition of the loss objective and the fact that  $\mathbf{a}$  is an optimal and, therefore, also feasible solution, we have  $\mathbf{a} \in B(\mathbf{b}, r\sigma_T)$  and thus  $\|\mathbf{a} - \mathbf{b}\|_2 \leq r\sigma_T$ .

Using the density function of the normal distribution, we can now write

$$\begin{aligned} & \mathbb{E}_{\mathbf{x} \sim q(\mathbf{x})} \left[ \log \left( \frac{q(\mathbf{x})}{p_{\xi^*}(\mathbf{x})} \right) \right] \\ &= \mathbb{E}_{\mathbf{x} \sim q(\mathbf{x})} \left[ \log \left( \frac{\mathcal{N}(\mathbf{b}) \left| \det \frac{d\Psi_*(\mathbf{b})}{d\mathbf{b}} \right|^{-1}}{\mathcal{N}(\mathbf{a}) \left| \det \frac{d\Psi_{\xi^*}(\mathbf{a})}{d\mathbf{a}} \right|^{-1}} \right) \right] \\ &= \mathbb{E}_{\mathbf{x} \sim q(\mathbf{x})} \left[ \log(\mathcal{N}(\mathbf{b})) + \log \left( \left| \det \frac{d\Psi_*(\mathbf{b})}{d\mathbf{b}} \right|^{-1} \right) - \log(\mathcal{N}(\mathbf{a})) - \log \left( \left| \det \frac{d\Psi_{\xi^*}(\mathbf{a})}{d\mathbf{a}} \right|^{-1} \right) \right] \\ &= \mathbb{E}_{\mathbf{x} \sim q(\mathbf{x})} [\log(\mathcal{N}(\mathbf{b})) - \log(\mathcal{N}(\mathbf{a}))] + \mathbb{E}_{\mathbf{x} \sim q(\mathbf{x})} \left[ \log \left( \left| \det \frac{d\Psi_*(\mathbf{b})}{d\mathbf{b}} \right|^{-1} \right) - \log \left( \left| \det \frac{d\Psi_{\xi^*}(\mathbf{a})}{d\mathbf{a}} \right|^{-1} \right) \right] \\ &= \mathbb{E}_{\mathbf{x} \sim q(\mathbf{x})} \left[ \log \left( \frac{\prod_{i=1}^d \frac{1}{\sigma_T \sqrt{2\pi}} \exp \left( -\frac{1}{2} \frac{b_i^2}{\sigma_T^2} \right)}{\prod_{i=1}^d \frac{1}{\sigma_T \sqrt{2\pi}} \exp \left( -\frac{1}{2} \frac{a_i^2}{\sigma_T^2} \right)} \right) \right] + \mathbb{E}_{\mathbf{x} \sim q(\mathbf{x})} \left[ \log \left( \left| \det \frac{d\Psi_{\xi^*}(\mathbf{a})}{d\mathbf{a}} \right| \right) - \log \left( \left| \det \frac{d\Psi_*(\mathbf{b})}{d\mathbf{b}} \right| \right) \right] \end{aligned} \tag{6}$$

with  $\Psi_{\xi^*}^{-1}(\mathbf{x}) = \mathbf{a}$  and  $\Psi_*^{-1}(\mathbf{x}) = \mathbf{b}$ .

Now, simplifying the left expression from above, we obtain

$$\mathbb{E}_{\mathbf{x} \sim q(\mathbf{x})} \left[ \log \left( \frac{\prod_{i=1}^d \frac{1}{\sigma_T \sqrt{2\pi}} \exp \left( -\frac{1}{2} \frac{b_i^2}{\sigma_T^2} \right)}{\prod_{i=1}^d \frac{1}{\sigma_T \sqrt{2\pi}} \exp \left( -\frac{1}{2} \frac{a_i^2}{\sigma_T^2} \right)} \right) \right] = \mathbb{E}_{\mathbf{x} \sim q(\mathbf{x})} \left[ \frac{1}{2\sigma_T^2} \sum_{i=1}^d (a_i^2 - b_i^2) \right].$$

Rewriting  $a_i = b_i + \epsilon_i$  for  $\epsilon_i \in \mathbb{R}$  we have

$$\mathbb{E}_{\mathbf{x} \sim q(\mathbf{x})} \left[ \frac{1}{2\sigma_T^2} \sum_{i=1}^d (2\epsilon_i b_i + \epsilon_i^2) \right] = \frac{1}{\sigma_T^2} \mathbb{E}_{\mathbf{x} \sim q(\mathbf{x})} \left[ \sum_{i=1}^d \epsilon_i b_i \right] + \frac{1}{2\sigma_T^2} \mathbb{E}_{\mathbf{x} \sim q(\mathbf{x})} \left[ \sum_{i=1}^d \epsilon_i^2 \right].$$

Since  $\|\mathbf{a} - \mathbf{b}\|_2 \leq r\sigma_T$ , we have that  $\sum_{i=1}^d (a_i - b_i)^2 \leq r^2 \sigma_T^2$  and again with  $a_i = b_i + \epsilon_i$  we have that  $\sum_{i=1}^d \epsilon_i^2 \leq r^2 \sigma_T^2$ .

Hence, we have that

$$\frac{1}{2\sigma_T^2} \mathbb{E}_{\mathbf{x} \sim q(\mathbf{x})} \left[ \sum_{i=1}^d \epsilon_i^2 \right] \leq \frac{1}{2\sigma_T^2} \mathbb{E}_{\mathbf{x} \sim q(\mathbf{x})} [r^2 \sigma_T^2] = \frac{r^2}{2},$$



where the last equality follows from the independence of the random variables in the multivariate distribution. Moreover, applying the Cauchy-Schwarz inequality, we have:

$$\begin{aligned}
\frac{1}{\sigma_T^2} \mathbb{E}_{\mathbf{x} \sim q(\mathbf{x})} \left[ \sum_{i=1}^d \epsilon_i b_i \right] &\leq \frac{1}{\sigma_T^2} \mathbb{E}_{\mathbf{x} \sim q(\mathbf{x})} \left[ \left( \sum_{i=1}^d \epsilon_i^2 \right)^{1/2} \left( \sum_{i=1}^d b_i^2 \right)^{1/2} \right] \\
&\leq \frac{1}{\sigma_T^2} \mathbb{E}_{\mathbf{x} \sim q(\mathbf{x})} \left[ r \sigma_T \left( \sum_{i=1}^d b_i^2 \right)^{1/2} \right] \\
&= \frac{r}{\sigma_T} \mathbb{E}_{\mathbf{b} \sim \mathcal{N}(\mathbf{0}, \sigma^2 \mathbf{I})} \left[ \left( \sum_{i=1}^d b_i^2 \right)^{1/2} \right],
\end{aligned} \tag{7}$$

where the second inequality follows from the definition of  $r$ . Since  $b_i \stackrel{\text{i.i.d.}}{\sim} \mathcal{N}(0, \sigma^2)$ , the sum of squares follows a Chi-squared distribution scaled by  $\sigma_T^2$  (i.e.,  $\sum_{i=1}^d b_i^2 \sim \sigma_T^2 \chi_d^2$ ). Thus:

$$\frac{r}{\sigma_T} \mathbb{E} \left[ \left( \sum_{i=1}^d b_i^2 \right)^{1/2} \right] = \frac{r}{\sigma_T} \mathbb{E} \left[ \sqrt{\sigma_T^2 \chi_d^2} \right] = \frac{r}{\sigma_T} \sigma_T \mathbb{E} \left[ \sqrt{\chi_d^2} \right] = r \sqrt{2} \frac{\Gamma(\frac{d+1}{2})}{\Gamma(\frac{d}{2})}.$$

To this end, applying Gautschi's inequality, we have:

$$\frac{\Gamma(\frac{d+1}{2})}{\Gamma(\frac{d}{2})} \leq \sqrt{\frac{d+1}{2}},$$

which gives:

$$r \sqrt{2} \frac{\Gamma(\frac{d+1}{2})}{\Gamma(\frac{d}{2})} \leq r \sqrt{2} \sqrt{\frac{d+1}{2}} = r \sqrt{d+1}.$$

Thus, the first term of Equation (6) is upper bounded by:

$$D_{\text{KL}}(q(\mathbf{x}) \parallel p_{\xi^*}(\mathbf{x})) \leq \frac{r^2}{2} + r \sqrt{2} \frac{\Gamma(\frac{d+1}{2})}{\Gamma(\frac{d}{2})} < \frac{r^2}{2} + r \sqrt{d+1}.$$

Combining with the second term of Equation (6), we get the final bound:

$$D_{\text{KL}}(q(\mathbf{x}) \parallel p_{\xi^*}(\mathbf{x})) \leq \frac{r^2}{2} + r \sqrt{d+1} + \mathbb{E}_{\mathbf{x} \sim q(\mathbf{x})} [|C(\Psi_*(\mathbf{x})) - C(\Psi_{\xi^*}(\mathbf{x}))|],$$

where  $C(\Psi_{\xi^*}(\mathbf{x})) = \log |\det J_{\Psi_{\xi^*}}(\Psi_{\xi^*}^{-1}(\mathbf{x}))|$ .

□

## A.2 Empirical measurement of the bound.

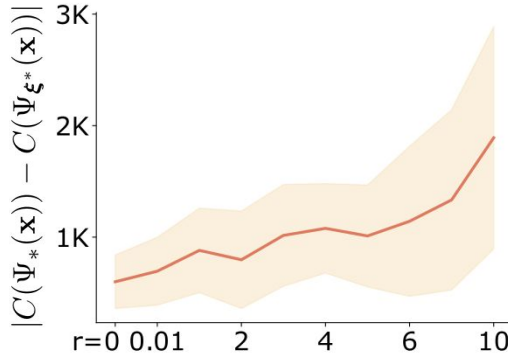


Figure 8: Estimation of  $|C(\Psi_*(\mathbf{x})) - C(\Psi_{\xi^*}(\mathbf{x}))|$  across various  $r$  values.

We can compute the first two terms of the KD bound in Theorem 1 since we know  $r$  and  $d$ . Although it would be hard to establish a tight analytic bound for the third term, we can still empirically estimate its magnitude in practical situations.

We test the empirical effect of  $r$  on the CIFAR10 [13] dataset. We change  $r$  from 10.0 down to 0.0 and approximate  $|C(\Psi_*(\mathbf{x})) - C(\Psi_{\xi^*}(\mathbf{x}))|$  by first sampling  $\mathbf{b} \sim \mathcal{N}(\mathbf{0}, \sigma_T^2 \mathbf{I})$ . We then approximate

$$C(\Psi_*(\mathbf{x})) \approx -\log \left( \left| \det \frac{d\Psi_*(\mathbf{b})}{d\mathbf{b}} \right| \right)$$

using a teacher solver  $\Psi_*(\cdot)$ , here the Uni\_PC solver with 20 NFE. Next we randomly sample an  $\mathbf{a} \in B(\mathbf{b}, r\sigma_T)$ , to approximate

$$C(\Psi_{\xi^*}(\mathbf{x})) \approx -\log \left( \left| \det \frac{d\Psi_{\xi^*}(\mathbf{a})}{d\mathbf{a}} \right| \right)$$

with the student solver  $\Psi_{\xi^*}(\cdot)$ , here the Uni\_PC solver with 7 NFE. Finally, we take the absolute difference

$$H(\mathbf{x}) := |C(\Psi_*(\mathbf{x})) - C(\Psi_{\xi^*}(\mathbf{x}))| = \left| \log \left( \left| \det \frac{d\Psi_{\xi^*}(\mathbf{a})}{d\mathbf{a}} \right| \right) - \log \left( \left| \det \frac{d\Psi_*(\mathbf{b})}{d\mathbf{b}} \right| \right) \right|.$$

Since the computation of the Jacobian is very slow, we repeat this for 100 samples and take the average to approximate  $\mathbb{E}_{\mathbf{x} \sim q(\mathbf{x})}[H(\mathbf{x})]$ , which is the third term of the bound in Theorem 1. Figure 8 shows how  $\mathbb{E}_{\mathbf{x} \sim q(\mathbf{x})}[H(\mathbf{x})]$  evolves as  $r$  changes. We observe that as  $r$  decreases so does  $\mathbb{E}_{\mathbf{x} \sim q(\mathbf{x})}[H(\mathbf{x})]$ . Hence, we empirically verified that the overall bound in Theorem 1 tightens with smaller  $r$  as desired. However, we also observe that  $\mathbb{E}_{\mathbf{x} \sim q(\mathbf{x})}[H(\mathbf{x})]$  does not converge to 0 for  $r \rightarrow 0$ . We hypothesize that this is related to the fact that we only compute an approximation of  $\mathbb{E}_{\mathbf{x} \sim q(\mathbf{x})}[H(\mathbf{x})]$  for randomly sampled  $\mathbf{a}$  and  $\mathbf{b}$  with a maximum L2 distance of  $r$  and not for  $\mathbf{a}$  and  $\mathbf{b}$  for which we have that  $\Psi_{\xi^*}(\mathbf{a}) = \Psi_*(\mathbf{b})$  as assumed by the theorem.

## B Experiment Details

In this section, we provide more experiment details for each setting, including the codebases and the configurations for evaluation.

### B.1 Practical Implement Details

We denote  $W$ ,  $H$ , and  $C$  as the width, height, and number of channels of an image, respectively. Thus we have  $d = C \times W \times H$ . Similarly,  $W'$ ,  $H'$ , and  $C'$  represent the corresponding dimensions in the latent space for the Latent Diffusion model [27], so  $d = C' \times W' \times H'$ .

**Teacher Solver and Data Generation.** Generally, we select the best-performing solver at 20 NFE as our teacher solver, except for ImageNet and text-to-image generation tasks. For ImageNet, we select 10 NFE as the teacher because it performs better than higher NFE, as noted in [29]. For text-to-image generation, we also use 10 NFE, since increasing NFE does not significantly enhance our model’s performance. We generate 50 to 100 samples for training. Detailed choices of solvers and NFE for the teacher solver are provided in Appendices B.1.1 to B.1.3.

**Optimizer and Trainable Parameters.** We update three primary parameter sets during training: the step-size parameters  $\xi$ , the coupling time step input to the denoising model  $\xi^c$ , and the starting point  $\mathbf{x}'_T$ . Their optimizers are RMSprop for  $\xi$  and SGD for both  $\xi^c$  and  $\mathbf{x}'_T$ . The learning rates are denoted as  $l_\xi$ ,  $l_{\xi^c}$ , and  $l_{\mathbf{x}'_T}$ . We set  $l_\xi = 0.005$  for pixel space datasets and  $l_\xi = 0.001$  for latent space datasets, while  $l_{\xi^c}$  and  $l_{\mathbf{x}'_T}$  are NFE-dependent. Further details are available in Appendices B.1.1 to B.1.3.

**Initialization.** We evaluate several baseline heuristics for  $\xi$  by computing their validation loss (a process taking only a few seconds) and choose the one that minimizes this loss for parameter initialization. We initialize  $\xi^c$  as a zero vector.

**Training.** Initially, we freeze  $\xi^c$  and optimize only  $\xi$  and  $\mathbf{x}'_T$  during the first one or two epochs (we call it phase 1). After this phase, we jointly update all parameters (we call it phase 2). At the end of each epoch, we update  $\mathbf{x}'_T$  for all samples in the validation set, without updating  $\xi$  and  $\mathbf{x}'_T$ , with respect to  $\mathcal{L}_{\text{soft}}$ . We save the checkpoint that minimizes  $\mathcal{L}_{\text{soft}}$  for the validation set after each training iteration.

**Evaluation.** We evaluate our model using the FID score with 50,000 randomly generated samples. For ImageNet, we generate an equal number of samples for each class to ensure a balanced FID evaluation.

We provide more detail about our training setting in Appendices B.1.1 to B.1.3.

### B.1.1 Pixel space diffusion on CIFAR10, FFHQ, and AFHQv2

- **Pre-trained model:**
  - EDM [10]
- **Image resolution:**
  - $W = H = 32, C = 3$  for CIFAR10.
  - $W = H = 64, C = 3$  for FFHQ and AFHQv2.
- **Training/Validation data:**
  - Size: 50/50.
  - The data are generated with the best baseline at NFE of 20, which is Uni\_PC solver with Time LogSNR discretization for all three datasets.
- **Phase 1 and Phase 2:**
  - Phase 1: 2 epochs.
  - Phase 2: 5 epochs.
- **Starting point  $\mathbf{x}'_T$  and  $r$ :**
  - SGD optimizer,  $l_{\mathbf{x}'_T} = \frac{12.0}{NFE}$ , momentum = 0, weight decay = 0.
  - $r = \frac{0.001 \times W \times H \times C}{NFE^2}$ .
- **Time discretization parameters  $\xi$** 
  - RMSprop optimizer,  $l_{\xi} = 0.005$ , momentum = 0.9, weight decay = 0.
  - Gradients are clipped by the norm of 1.0.
  - If the validation loss does not improve for 5 consecutive iterations (patience = 5), reduce the learning rate by a factor of 0.8. Stop decay if the learning rate reaches a minimum of  $5 \times 10^{-5}$ .
- **Time coupling parameters  $\xi^c$ :**
  - SGD optimizer,  $l_{\xi^c} = \frac{0.1}{NFE}$ .
  - Gradients are clipped by the norm of 1.0.
  - If the validation loss does not improve for 5 consecutive iterations (patience = 5), reduce the learning rate by a factor of 0.8. Stop decay if the learning rate reaches a minimum of  $1 \times 10^{-6}$ .

### B.1.2 Latent space diffusion on LSUN-Bedroom and ImageNet

- **Pre-trained model:**
  - Latent Diffusion [27]
- **Image resolution:**
  - $W = H = 256, C = 3$ .
  - $W' = H' = 64, C' = 3$ .
- **Guidance scale:** 2.0 (for ImageNet).
- **Training/Validation data:**

- Size: 50/50.
- The data are generated with the best baseline at NFE of 20, which is Uni\_PC solver with Time uniform discretization for both datasets.
- **Phase 1 and Phase 2:**
  - Phase 1: 2 epochs.
  - Phase 2: 5 epochs.
- **Starting point  $\mathbf{x}'_T$  and  $r$ :**
  - SGD optimizer,  $l_{\mathbf{x}'_T} = \frac{12.0}{NFE}$ , momentum = 0, weight decay = 0.
  - $r = \frac{0.001 \times W \times H \times C}{NFE^2}$ .
- **Time discretization parameters  $\xi$** 
  - RMSprop optimizer,  $l_{\xi} = 0.001$ , momentum = 0.9, weight decay = 0.
  - Gradients are clipped by the norm of 1.0.
  - If the validation loss does not improve for 5 consecutive iterations (patience = 5), reduce the learning rate by a factor of 0.8. Stop decay if the learning rate reaches a minimum of  $5 \times 10^{-5}$ .
- **Time coupling parameters  $\xi^c$ :**
  - SGD optimizer,  $l_{\xi^c} = \frac{0.001}{NFE}$ .
  - Gradients are clipped by the norm of 1.0.
  - If the validation loss does not improve for 5 consecutive iterations (patience = 5), reduce the learning rate by a factor of 0.8. Stop decay if the learning rate reaches a minimum of  $1 \times 10^{-6}$ .

### B.1.3 Text-to-Image generation with Stable Diffusion

We randomly sample 5 captions from the MS COCO dataset [16], which are:

1. *"Two individuals learning to ski along with an instructor."*
2. *"A man sitting on a chair that is on a deck over the water."*
3. *"A dog sitting at a table in front of a plate."*
4. *"Four people sit around eating food outside together."*
5. *"A cat dips its paws into a cup on a nightstand."*

We utilize Stable Diffusion v1.4 [27] with the Uni\_PC (2M) solver and 10 NFE to generate 50 samples for training. The time discretization is trained with the same solver but with fewer NFE, specifically 6 and 7, in two different settings.

- **Pre-trained model:**
  - Stable Diffusion [27]
- **Image resolution:**
  - $W = H = 512, C = 3$ .
  - $W' = H' = 64, C' = 4$ .
- **Guidance scale:** 7.5.
- **Training/Validation data:**
  - Size: 25/25.
  - The data are generated at 10 NFE with Uni\_PC solver with Time uniform discretization.
- **Phase 1 and Phase 2:**
  - Phase 1: 2 epochs.
  - Phase 2: 5 epochs.
- **Starting point  $\mathbf{x}'_T$  and  $r$ :**
  - SGD optimizer,  $l_{\mathbf{x}'_T} = \frac{12.0}{NFE}$ , momentum = 0, weight decay = 0.

$$- r = \frac{0.001 \times W \times H \times C}{NFE^2}.$$

- **Time discretization parameters  $\xi$**

- RMSprop optimizer,  $l_\xi = 0.001$ , momentum = 0.9, weight decay = 0.
- Gradients are clipped by the norm of 1.0.
- If the validation loss does not improve for 5 consecutive iterations (patience = 5), reduce the learning rate by a factor of 0.8. Stop decay if the learning rate reaches a minimum of  $5 \times 10^{-5}$ .

- **Time coupling parameters  $\xi^c$ :**

- SGD optimizer,  $l_{\xi^c} = \frac{0.001}{NFE}$ .
- Gradients are clipped by the norm of 1.0.
- If the validation loss does not improve for 5 consecutive iterations (patience = 5), reduce the learning rate by a factor of 0.8. Stop decay if the learning rate reaches a minimum of  $1 \times 10^{-6}$ .

## B.2 Baseline discretization heuristics

We compare our learned time discretization with the following discretizations heuristics:

**Polynomial discretization (Time quadratic, Time uniform):** This discretization is a polynomial function. Specifically:

$$t_i = \left(\frac{i}{N}\right)^\rho (t_{\max} - t_{\min}) + t_{\min}, \quad t_{\max} = T, \quad i = 0, 1, \dots, N \quad (8)$$

here  $\rho$  is often set to 1 or 2 [7, 21, 31, 33] which corresponds to time quadratic and time uniform discretization.

**Time EDM discretization:** First introduced by [10], Time EDM discretization has been shown to be effective with Heun’s solver on EDM pre-trained model [10]:

$$\sigma(t_i) = \left(\sigma_{\max}^{-\rho} + \frac{i}{N-1} (\sigma_{\min}^{-\rho} - \sigma_{\max}^{-\rho})\right)^\rho \quad (9)$$

**Time LogSNR:** This schedule uniformly separate the logSNR. Specifically:

$$\lambda(t_i) = \frac{N-i}{N} (\lambda_{\max} - \lambda_{\min}) + \lambda_{\min}, \quad \text{where } \lambda(t_i) = \frac{\alpha(t_i)}{\sigma(t_i)} \quad (10)$$

this schedule is often used with solvers from [20, 21, 42].

## B.3 The Rematerialization Trick

Although the student model has few trainable parameters, the memory cost of maintaining the forward pass state scales linearly with the number of inference steps when taking gradients concerning model samples. This scaling can quickly become unfeasible given the large size of DPM architectures. To address this, we adopt the gradient rematerialization technique proposed in [34], following [14]. Rather than storing specific forward pass outputs for backward pass computations, we recompute them as needed, trading  $\mathcal{O}(N)$  memory cost for  $\mathcal{O}(N)$  computation time. This involves rematerializing calls to the pre-trained DDPM while keeping all progressively denoised images from the sampling chain in memory. Our model exhibits rapid convergence, even with a small batch size of 1 or 2.

## C Additional Results

### C.1 Compare to AYS on CIFAR10 and FFHQ

Table 5: Comparison of LD3 to AYS [29] (results sourced from [29]) and the best baseline (Best) among *time uniform*, *time quadratic*, *time EDM*, and *time LogSNR*. Unlike the experiments in Figure 5, which use DPM\_Solver++ (3M) (order = 3), we use DPM\_Solver++ (2M) (order = 2) following [29].

Pre-trained DPM [10]	CIFAR10		FFHQ	
NFE	10	20	10	20
DPM_Solver++ (2M) (Best)	5.07	2.37	7.07	3.41
DPM_Solver++ (2M) (AYS)	<b>2.98</b>	<b>2.10</b>	5.43	3.29
DPM_Solver++ (2M) LD3	<b>3.38 ± 0.64</b>	2.36 ± 0.02	<b>3.98 ± 0.10</b>	<b>2.89 ± 0.03</b>

### C.2 FID Progression during training

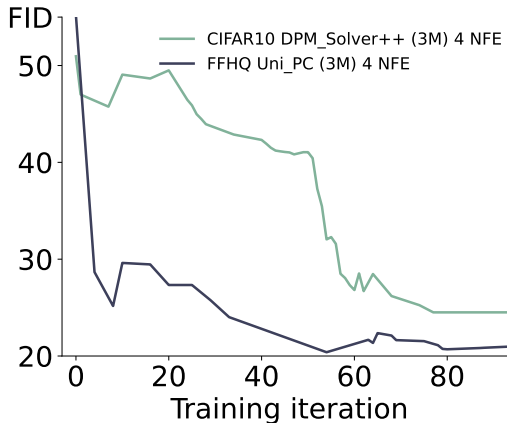


Figure 9: **FID progression during training.** We report the FID values during training for CIFAR10 and FFHQ datasets, using 4 NFE with the DPM\_Solver++ (3M) for CIFAR10 and the Uni\_PC (3M) solver for FFHQ. The FID, computed based on 5000 generated samples, is evaluated each time the validation loss decreases.

In our method, we save the optimal parameters based on the validation loss criterion. Figure 9 shows a decreasing trend in FID values throughout the training process. This trend suggests a correlation between FID and validation loss, indicating that FID generally decreases as the validation loss decreases. This observation further validates the effectiveness of our method.



### C.3 Full result tables

Table 6: Full FID comparison on CIFAR10  $32 \times 32$  [13].

Solver	Discretization	NFE								
		4	5	6	7	8	9	10	14	20
Euler	Time LogSNR	73.77	54.50	39.14	30.69	24.14	20.31	16.68	10.36	6.62
	Time Uniform	283.46	264.68	250.99	239.97	229.95	220.60	211.73	179.23	141.83
	Time Quadratic	179.75	139.70	108.13	86.05	69.28	57.06	48.39	29.31	19.01
	Time EDM	67.82	50.66	36.53	28.79	23.14	19.30	16.48	10.23	6.70
	LD3	<b>25.78 ± 1.46</b>	<b>20.37 ± 3.92</b>	<b>12.90 ± 0.24</b>	<b>10.63 ± 0.03</b>	<b>8.37 ± 0.12</b>	<b>7.75 ± 0.31</b>	<b>7.05 ± 0.45</b>	<b>5.26 ± 0.05</b>	<b>4.03 ± 0.20</b>
Uni_FC (3M)	Time LogSNR	43.92	24.01	13.12	6.63	4.41	3.55	3.16	<b>2.20</b>	<b>2.08</b>
	Time Uniform	282.77	263.61	249.42	237.81	227.21	217.09	207.40	171.38	130.57
	Time Quadratic	164.78	117.28	85.14	65.25	51.91	42.48	35.52	20.26	13.00
	Time EDM	50.65	34.24	19.56	12.68	9.65	7.83	6.12	3.77	2.27
	LD3	<b>17.68 ± 3.99</b>	<b>9.09 ± 3.27</b>	<b>4.24 ± 0.52</b>	<b>2.68 ± 0.03</b>	<b>3.53 ± 0.16</b>	<b>3.07 ± 0.03</b>	<b>2.90 ± 0.07</b>	<b>2.21 ± 0.02</b>	<b>2.08 ± 0.00</b>
DPM_Solver++ (3M)	Time LogSNR	46.59	24.99	12.16	6.88	4.62	3.54	<b>3.08</b>	<b>2.32</b>	<b>2.12</b>
	Time Uniform	282.94	263.80	249.75	238.26	227.79	217.86	208.34	172.99	132.71
	Time Quadratic	170.95	124.73	91.56	69.93	54.97	44.59	37.21	21.26	13.23
	Time EDM	50.91	32.13	18.64	11.71	8.44	6.51	5.16	2.95	2.27
	LD3	<b>20.05 ± 1.41</b>	<b>11.20 ± 2.38</b>	<b>6.18 ± 1.44</b>	<b>3.19 ± 0.05</b>	<b>3.84 ± 0.62</b>	<b>3.21 ± 0.22</b>	<b>3.18 ± 0.16</b>	<b>2.43 ± 0.11</b>	<b>2.12 ± 0.03</b>
iPNDM (3M)	Time LogSNR	35.04	20.52	11.80	7.69	5.67	4.37	3.69	2.53	2.19
	Time Uniform	266.26	242.94	229.39	217.13	205.24	194.72	185.28	148.13	111.95
	Time Quadratic	139.72	96.67	68.82	52.32	37.82	27.51	23.40	14.69	9.18
	Time EDM	29.78	17.35	9.95	7.61	5.41	5.00	3.80	3.22	2.80
	LD3	<b>12.61 ± 1.65</b>	<b>6.66 ± 0.05</b>	<b>4.52 ± 0.37</b>	<b>3.57 ± 0.30</b>	<b>3.03 ± 0.48</b>	<b>2.73 ± 0.06</b>	<b>2.50 ± 0.04</b>	<b>2.26 ± 0.04</b>	<b>2.15 ± 0.01</b>

Table 7: Full FID comparison on AFHQv2  $64 \times 64$  [1].

Solver	Discretization	NFE								
		4	5	6	7	8	9	10	14	20
Euler	Time LogSNR	39.03	31.79	22.24	16.83	14.18	12.09	10.36	6.81	4.73
	Time Uniform	153.33	143.69	135.04	126.40	117.85	109.34	101.11	73.09	47.02
	Time Quadratic	73.35	46.51	34.33	28.10	24.21	21.57	19.60	14.71	10.96
	Time EDM	29.14	22.96	17.57	14.09	11.92	10.23	9.01	6.24	4.52
	LD3	<b>24.70 ± 2.29</b>	<b>17.57 ± 1.35</b>	<b>12.06 ± 0.10</b>	<b>10.20 ± 0.58</b>	<b>7.80 ± 0.46</b>	<b>5.95 ± 0.05</b>	<b>6.04 ± 0.31</b>	<b>4.15 ± 0.07</b>	<b>3.14 ± 0.17</b>
Uni_FC (3M)	Time LogSNR	33.78	13.01	8.27	5.07	4.60	4.46	3.81	<b>2.35</b>	<b>2.11</b>
	Time Uniform	153.24	143.46	134.27	124.98	115.52	106.21	97.30	67.71	41.87
	Time Quadratic	66.38	41.56	30.62	24.26	20.47	18.04	16.33	12.73	9.58
	Time EDM	23.74	15.84	10.24	8.37	7.75	6.67	6.26	3.57	2.26
	LD3	<b>11.52 ± 0.88</b>	<b>6.13 ± 0.15</b>	<b>4.43 ± 0.58</b>	<b>2.84 ± 0.10</b>	<b>2.60 ± 0.08</b>	<b>2.62 ± 0.09</b>	<b>2.87 ± 0.24</b>	<b>2.36 ± 0.01</b>	<b>2.11 ± 0.00</b>
DPM_Solver++ (3M)	Time LogSNR	27.82	17.88	10.72	6.15	4.28	3.64	3.19	<b>2.37</b>	2.24
	Time Uniform	153.20	143.45	134.46	125.39	116.13	107.01	98.25	68.80	42.85
	Time Quadratic	68.78	42.48	30.92	24.70	20.94	18.48	16.73	12.79	9.74
	Time EDM	19.65	13.34	9.64	7.82	6.54	4.99	4.11	2.90	2.28
	LD3	<b>14.38 ± 0.69</b>	<b>7.94 ± 0.68</b>	<b>5.74 ± 1.46</b>	<b>3.93 ± 0.20</b>	<b>3.12 ± 0.16</b>	<b>2.88 ± 0.17</b>	<b>2.90 ± 0.25</b>	2.52 ± 0.02	<b>2.15 ± 0.02</b>
iPNDM (3M)	Time LogSNR	23.20	15.63	9.55	5.98	4.49	3.75	3.19	2.41	2.17
	Time Uniform	159.22	139.47	125.17	113.68	102.99	92.57	82.89	54.39	33.33
	Time Quadratic	53.67	32.27	23.80	20.32	18.18	16.52	15.10	10.30	6.89
	Time EDM	15.35	9.01	6.26	4.73	3.83	3.55	3.02	2.65	2.37
	LD3	<b>10.38 ± 0.27</b>	<b>5.43 ± 0.24</b>	<b>3.84 ± 0.32</b>	<b>2.74 ± 0.16</b>	<b>2.45 ± 0.08</b>	<b>2.40 ± 0.19</b>	<b>2.23 ± 0.05</b>	<b>2.14 ± 0.02</b>	<b>2.12 ± 0.01</b>

Table 8: Full FID comparison on FFHQ 64×64 [11].

Solver	Discretization	NFE								
		4	5	6	7	8	9	10	14	20
Euler	Time LogSNR	63.39	50.22	39.94	32.57	27.43	23.53	20.57	13.48	9.05
	Time Uniform	179.84	166.68	155.21	144.98	135.76	127.43	119.97	96.98	75.57
	Time Quadratic	100.77	79.58	65.48	55.43	48.00	42.37	37.97	27.51	19.96
	Time EDM	57.39	43.95	35.19	28.97	24.52	21.18	18.51	12.41	8.45
	LD3	<b>38.01 ± 2.85</b>	<b>28.52 ± 2.18</b>	<b>24.01 ± 3.59</b>	<b>19.08 ± 1.19</b>	<b>15.91 ± 0.72</b>	<b>12.98 ± 0.74</b>	<b>11.52 ± 0.50</b>	<b>7.26 ± 0.32</b>	<b>5.12 ± 0.12</b>
Uni_PC (3M)	Time LogSNR	53.25	20.20	11.24	7.09	5.59	4.53	3.90	2.89	<b>2.54</b>
	Time Uniform	178.68	165.03	152.97	142.09	132.22	123.28	115.20	90.29	67.58
	Time Quadratic	89.75	65.94	51.28	41.47	34.67	29.85	26.45	19.36	14.92
	Time EDM	47.74	26.73	15.18	11.33	11.70	10.94	8.93	3.71	2.85
	LD3	<b>18.72 ± 1.27</b>	<b>10.56 ± 0.72</b>	<b>5.99 ± 0.07</b>	<b>4.23 ± 0.18</b>	<b>3.85 ± 0.64</b>	<b>3.60 ± 0.15</b>	<b>3.59 ± 0.28</b>	<b>2.72 ± 0.06</b>	<b>2.54 ± 0.00</b>
DPM_Solver++ (3M)	Time LogSNR	46.14	22.79	14.01	8.63	6.18	4.86	4.18	3.18	2.73
	Time Uniform	179.07	165.50	153.56	142.80	133.07	124.26	116.30	91.70	69.10
	Time Quadratic	94.11	70.17	54.93	44.64	37.41	32.12	28.30	20.26	15.15
	Time EDM	39.59	23.81	15.29	11.17	9.67	8.45	7.01	3.50	2.70
	LD3	<b>27.63 ± 0.23</b>	<b>14.01 ± 0.97</b>	<b>7.67 ± 0.60</b>	<b>5.24 ± 0.20</b>	<b>4.67 ± 0.09</b>	<b>3.81 ± 0.16</b>	<b>3.52 ± 0.10</b>	<b>2.85 ± 0.05</b>	<b>2.65 ± 0.03</b>
iPNDM (3M)	Time LogSNR	36.54	24.57	16.44	11.31	8.11	6.39	5.39	3.85	2.88
	Time Uniform	39.49	26.15	20.80	17.52	14.69	12.50	10.89	7.05	4.48
	Time Quadratic	71.51	51.66	39.17	31.32	26.50	23.71	21.22	16.78	12.13
	Time EDM	29.35	17.52	11.44	8.76	6.86	5.96	4.93	3.68	3.06
	LD3	<b>16.88 ± 1.51</b>	<b>11.07 ± 0.67</b>	<b>6.63 ± 0.50</b>	<b>5.00 ± 0.20</b>	<b>3.98 ± 0.27</b>	<b>3.50 ± 0.20</b>	<b>3.25 ± 0.12</b>	<b>2.85 ± 0.11</b>	<b>2.67 ± 0.05</b>

Table 9: Full FID comparison on LSUN-Bedroom 256×256 [37].

Solver	Discretization	NFE							
		4	5	6	7	8	9	10	
Uni_PC (2M)	Time LogSNR	73.87	34.06	17.18	12.05	10.07	8.67	7.72	
	Time Uniform	39.78	13.88	6.57	4.56	<b>3.96</b>	3.74	<b>3.54</b>	
	Time Quadratic	35.97	15.94	10.91	9.43	8.87	8.28	7.42	
	Time EDM	297.83	259.90	232.79	204.89	177.79	151.45	129.82	
	LD3	<b>20.15 ± 1.10</b>	<b>9.09 ± 0.42</b>	<b>4.98 ± 0.10</b>	<b>4.18 ± 0.15</b>	<b>4.01 ± 0.05</b>	<b>3.61 ± 0.04</b>	<b>3.60 ± 0.08</b>	
DPM_Solver++ (2M)	Time LogSNR	80.44	35.81	16.95	11.38	9.69	8.81	8.19	
	Time Uniform	48.82	18.64	8.50	5.16	4.24	<b>3.84</b>	<b>3.62</b>	
	Time Quadratic	47.64	21.29	12.42	9.68	8.90	8.58	8.09	
	Time EDM	324.41	294.61	268.96	243.91	216.80	191.55	168.77	
	LD3	<b>28.83 ± 0.16</b>	<b>12.17 ± 0.68</b>	<b>5.83 ± 0.15</b>	<b>4.16 ± 0.04</b>	<b>3.71 ± 0.03</b>	<b>3.77 ± 0.07</b>	3.81 ± 0.11	
iPNDM (2M)	Time LogSNR	55.77	32.51	20.26	14.52	11.61	9.76	8.25	
	Time Uniform	11.93	6.38	5.08	<b>4.39</b>	4.17	<b>3.81</b>	<b>3.69</b>	
	Time Quadratic	27.44	18.77	14.39	11.71	9.72	8.43	7.50	
	Time EDM	312.44	284.15	252.37	221.56	194.27	168.35	146.16	
	LD3	<b>8.48 ± 0.11</b>	<b>5.93 ± 0.11</b>	<b>4.52 ± 0.17</b>	<b>4.31 ± 0.17</b>	<b>3.87 ± 0.07</b>	<b>3.84 ± 0.07</b>	<b>3.59 ± 0.10</b>	

Table 10: Full FID comparison on ImageNet 256×256 [28].

Solver	Discretization	NFE							
		4	5	6	7	8	9	10	
Uni_PC (2M)	Time LogSNR	50.26	19.22	9.08	5.87	4.90	4.65	4.47	
	Time Uniform	20.01	8.51	5.92	5.20	5.00	5.04	5.01	
	Time Quadratic	30.66	13.71	7.15	5.17	4.61	<b>4.32</b>	<b>4.32</b>	
	Time EDM	235.31	218.15	203.26	186.88	171.76	157.77	145.08	
	LD3	<b>9.89 ± 0.06</b>	<b>5.03 ± 0.17</b>	<b>4.46 ± 0.06</b>	<b>4.32 ± 0.00</b>	<b>4.33 ± 0.07</b>	<b>4.27 ± 0.07</b>	<b>4.31 ± 0.01</b>	
DPM_Solver++ (2M)	Time LogSNR	54.61	23.24	11.52	7.26	5.70	5.01	<b>4.77</b>	
	Time Uniform	26.07	11.91	7.51	5.95	5.42	5.20	5.13	
	Time Quadratic	41.94	22.42	12.04	7.78	6.00	5.18	4.79	
	Time EDM	244.49	233.18	221.56	210.02	196.48	185.39	173.76	
	LD3	<b>16.92 ± 0.13</b>	<b>6.74 ± 0.05</b>	<b>4.74 ± 0.08</b>	<b>4.44 ± 0.05</b>	<b>4.37 ± 0.05</b>	<b>4.37 ± 0.06</b>	4.46 ± 0.03	
iPNDM (2M)	Time LogSNR	51.35	24.93	13.94	9.11	6.95	5.88	5.40	
	Time Uniform	13.86	7.80	6.03	5.35	5.10	4.97	4.97	
	Time Quadratic	28.54	15.98	9.50	6.76	5.56	4.98	4.66	
	Time EDM	237.68	223.29	210.10	195.59	182.85	169.36	157.31	
	LD3	<b>9.13 ± 0.20</b>	<b>6.03 ± 0.02</b>	<b>5.09 ± 0.04</b>	<b>4.68 ± 0.04</b>	<b>4.62 ± 0.07</b>	<b>4.57 ± 0.02</b>	<b>4.55 ± 0.03</b>	

#### C.4 Additional Samples

We offer additional visual examples in Figure 20 to illustrate the qualitative effectiveness of LD3. It's evident that the visual quality of LD3 surpasses discretization baselines. Our method can generate images with more visual details and less severe contrast.

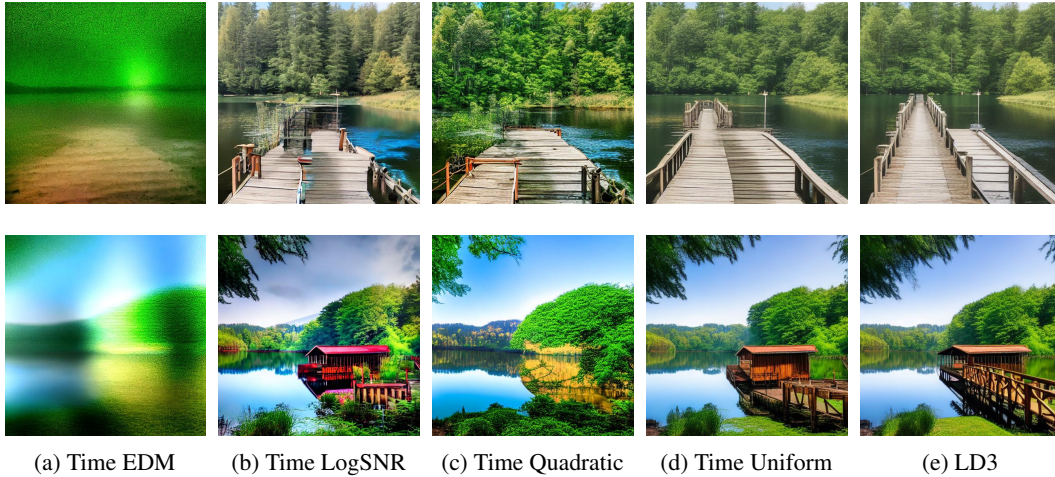


Figure 10: Text prompt: "A tranquil lake surrounded by lush greenery and a small wooden dock" Stable Diffusion v1.4 [27], Uni\_PC (2M) solver, NFE = 6.

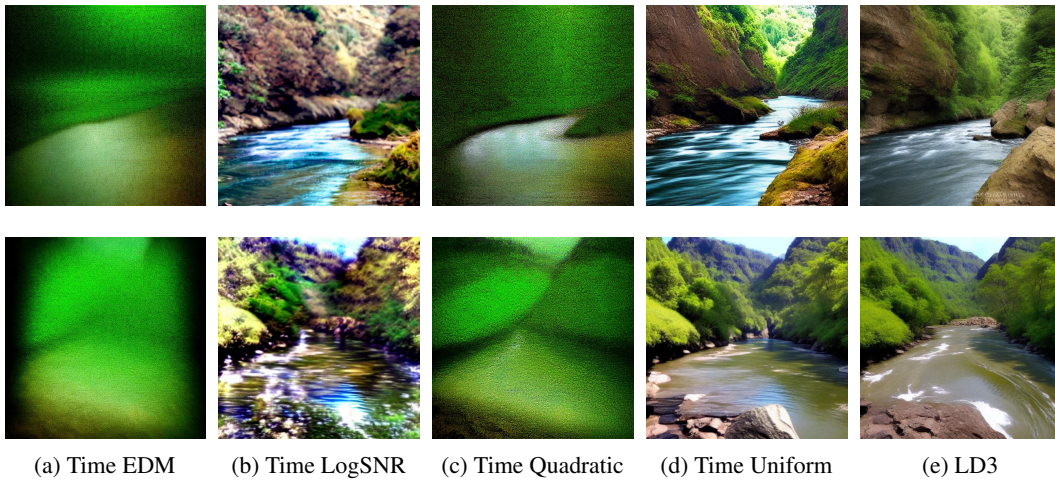


Figure 11: Text prompt: "A tranquil river winding through a lush valley, overlooked by rugged cliffs", Stable Diffusion v1.4 [27], Uni\_PC (2M) solver, NFE = 6.



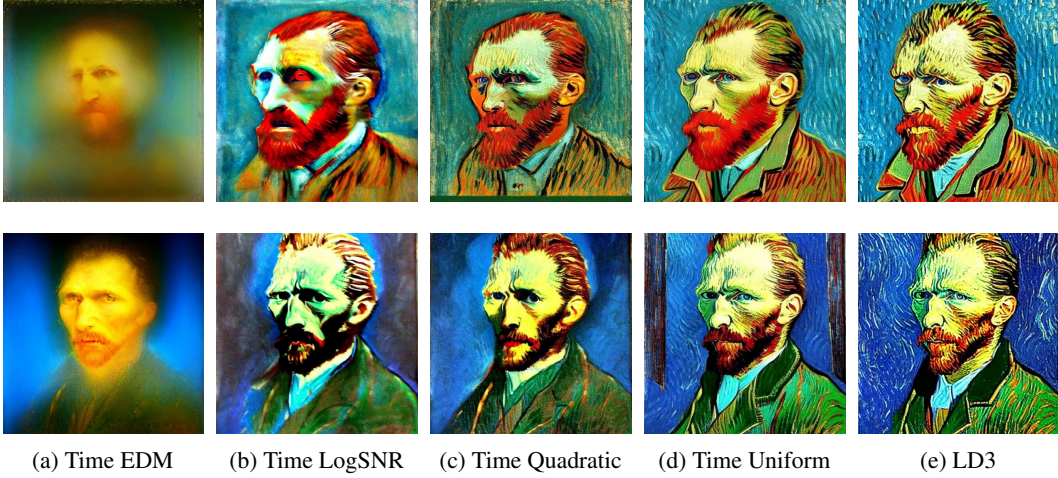


Figure 12: Text prompt: "Portrait of Van Gogh in his iconic style". Stable Diffusion v1.4 [27], Uni\_PC (2M), NFE = 7.

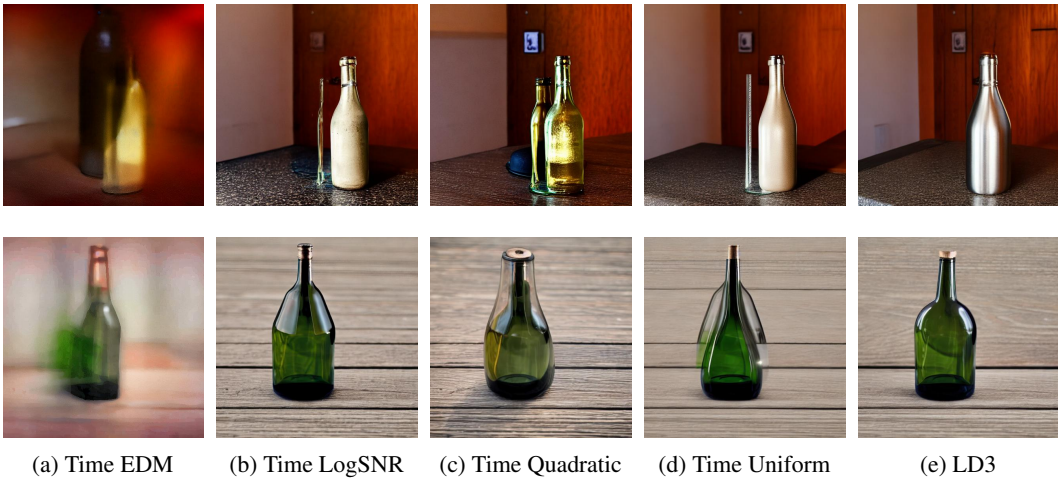


Figure 13: Text prompt: "A bottle on a table". Stable Diffusion v1.4 [27], Uni\_PC (2M), NFE = 7.



Figure 14: **Side-by-side comparison.** Random samples LSUN-Bedroom, iPNDM (2M), NFE = 4.



(a) Best baseline (Time quadratic), FID = 35.97

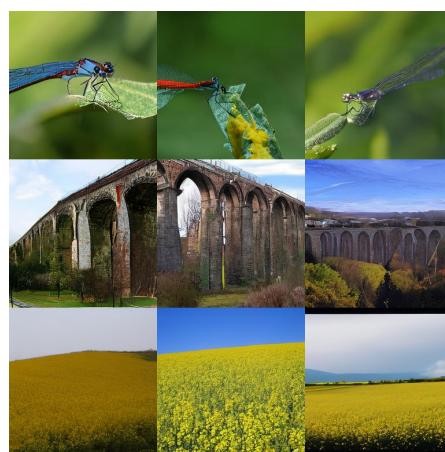


(b) LD3, FID = 20.91

Figure 15: **Side-by-side comparison.** Random samples on LSUN-Bedroom, Uni\_PC (2M), NFE = 4.



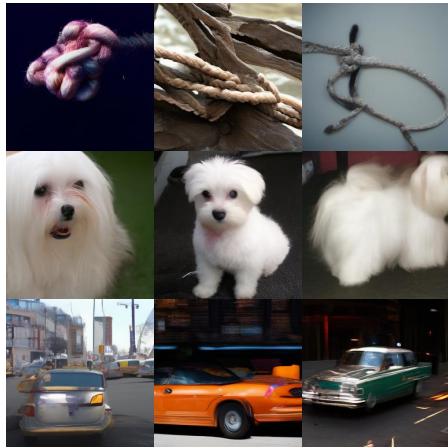
(a) Best baseline (Time uniform), FID = 5.42



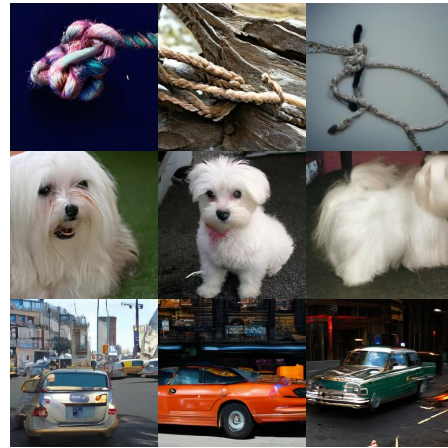
(b) LD3, FID = 4.31.

Figure 16: **Side-by-side comparison.** Random samples on class-conditional ImageNet. From top to bottom, the class labels are "Damselfly", "Viaduct", "Rapeseed", DPM\_Solver++ (2M), NFE = 8.





(a) Best baseline (Time uniform), FID = 5.92



(b) LD3, FID = 4.41.

Figure 17: **Side-by-side comparison.** Random samples on class-conditional ImageNet. From top to bottom, the class labels are "Knot", "Maltese dog", "Taxicab", Uni\_PC (2M), NFE = 6.



(a) Best baseline (logSNR), FID = 13.01



(b) LD3, FID = 6.02

Figure 18: **Side-by-side comparison.** Random samples on AFHQv2, Uni\_PC (3M), NFE = 5.



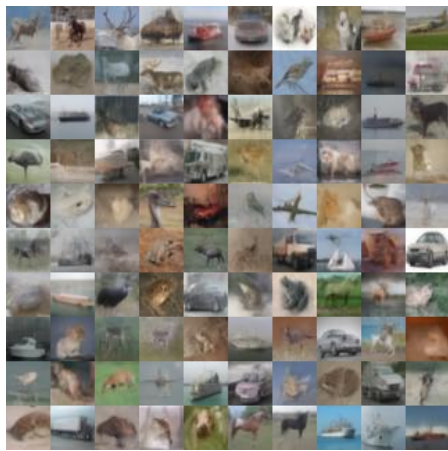
(a) Best baseline (Time EDM), FID = 47.74



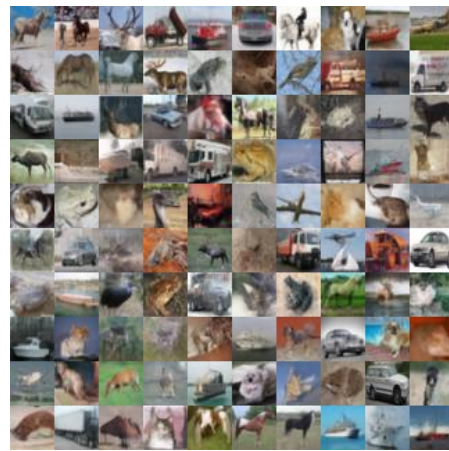
(b) LD3, FID = 19.46

Figure 19: **Side-by-side comparison.** Random samples on FFHQ, Uni\_PC (3M), NFE = 4.





(a) Best baseline (Time EDM), FID=36.53



(b) LD3, FID=13.02

Figure 20: **Side-by-side comparison.** Random samples on CIFAR10, Euler, NFE = 6.